

**FINITE-ELEMENT MODELLING
OF THE FLUID-STRUCTURE INTERACTION
BETWEEN THE EAR CANAL AND EARDRUM**

Jennifer L. Day

**A thesis submitted to the Faculty of Graduate Studies and
Research in partial fulfillment of the requirements
for the degree of Master of Engineering**

**Department of Electrical Engineering
McGill University
Montréal, Canada
October 1990**

© Jennifer L. Day, 1990

ABSTRACT

In this work mathematical modelling methods are formulated in order to examine how sound pressures in the ear canal interact with displacements on the eardrum. Existing finite-element code is altered and new code developed to deal with the acoustics of the ear canal and the mathematics of the fluid-structure interaction problem. A finite-element model of the human ear canal and eardrum using simplified geometry is developed as an initial approach to the coupled problem. The preliminary finite-element model consists of a cylindrical tube attached to a circular plate, with appropriate material properties assigned to each part. The coupled ear canal/eardrum problem is analyzed at several frequencies. Output is discussed in view of results obtained for eigenvalue analyses of both ear canal and eardrum as separate problems.

RÉSUMÉ

Dans cette étude, des méthodes de modélisation mathématique sont employées afin d'examiner l'interaction entre la pression sonore dans le canal auditif et les déplacements du tympan. Un logiciel d'éléments finis est modifié et de nouveaux algorithmes développés de façon à traiter l'acoustique du canal auditif et le problème de l'action réciproque fluide-solide. Un modèle d'éléments finis du canal auditif et du tympan humains employant une géométrie simplifiée est développé comme approche initiale au problème couplé. Le modèle préliminaire est constitué d'un tube cylindrique rattaché à une plaque circulaire auxquels sont assignés des propriétés des matériaux appropriées. Le problème couplé canal auditif/tympan est analysé à plusieurs fréquences. Les résultats de cette analyse sont éclairés par les solutions obtenues en traitant le canal auditif et le tympan en tant que problèmes séparés. La méthode des valeurs propres est utilisée à cet effet.

ACKNOWLEDGMENTS

I would like to thank my research director, Dr. W.R.J. Funnell, for all the supervision and guidance provided throughout the course of this thesis. His patience was greatly appreciated, in light of my interest in the courses offered by the Arts Department at McGill, as well as my endless questions pertaining to this work.

I also greatly appreciate the help and encouragement I have received from the students and staff of the Biomedical Engineering Department. These people and the special working environment make it difficult to imagine a better place to undertake graduate studies.

I am indebted to all my friends, who have shared discussions with me on film, literature and music, who have made things seem easier, and who have made me understand that we can and must change our lives.

Finally, I thank my parents and my aunt, for their constant care and support.

This research was supported by scholarships from NSERC and FCAR, and an operating grant from MRC.

TABLE OF CONTENTS

ABSTRACT	i
RÉSUMÉ	ii
ACKNOWLEDGMENTS	iii
TABLE OF CONTENTS	iv
LIST OF FIGURES	vii
LIST OF TABLES	viii
PRINCIPAL NOTATION	ix
CHAPTER 1 INTRODUCTION	1
CHAPTER 2 PHYSIOLOGY OF THE EXTERNAL AND MIDDLE EAR	
2.1 Introduction to the Hearing System	3
2.2 The External Ear	
2.2.1 The pinna	5
2.2.2 The ear canal	7
2.3 The Eardrum	9
2.4 The Middle Ear	11
CHAPTER 3 EXPERIMENTAL OBSERVATIONS AND MODELLING OF THE EXTERNAL AND MIDDLE EAR	
3.1 Introduction	15
3.2 The Ear Canal	
3.2.1 Sound-pressure experiments in the external ear	15
3.2.2 Energy reflectance studies	19
3.2.3 Network modelling of the ear canal	21
3.2.4 Studies focusing on ear-canal geometry	22

3.3	The Eardrum	
3.3.1	Experimental observation of eardrum vibrations	24
3.3.2	Theories and models of eardrum behaviour	27
3.4	The Middle Ear	
3.4.1	Experiments concerning vibration of the middle-ear ossicles	30
3.4.2	Middle-ear models	31
3.5	Modelling the Ear Canal/Eardrum Coupling	34
CHAPTER 4 FINITE-ELEMENT MODELLING		
4.1	Introduction	39
4.2	The Finite-Element Method	40
4.2.1	The variational formulation and the functional	42
4.2.2	Finite-element equilibrium equations	43
4.2.3	Element formulations	47
4.3	An Acoustic Analogy	54
4.4	Fluid-Structure Interaction	
4.4.1	Introduction	58
4.4.2	Approaches to the interaction problem	59
4.4.3	Solution of the fluid-structure problem using existing finite-element code	60
4.4.4	Implementing the fluid-structure coupling using SAP	67
4.4.5	Viewing the coupled results	69
4.4.6	Code validation	70
CHAPTER 5 FINITE-ELEMENT TESTS AND RESULTS		
5.1	Introduction	71
5.2	The Finite-Element Model of the Ear Canal and Eardrum	
5.2.1	Eardrum shape and properties	72
5.2.2	Ear canal shape and properties	72
5.2.3	Finite-element meshes for the eardrum and ear canal	73
5.3	Eigenvalue Analysis of the Uncoupled Problem	
5.3.1	The eardrum	75
5.3.2	The ear canal	79

5.4 Results for the coupled problem	
5.4.1 Introduction	82
5.4.2 Results at individual frequencies	82
CHAPTER 6 CONCLUSION	
6.1 Summary of Contributions	91
6.2 Future Work	91
6.3 Applications	93
REFERENCES	95

LIST OF FIGURES

Fig. 2.1 The human ear	4
Fig. 2.2 View of the external ear	6
Fig. 2.3 The human eardrum	
(a) Sketch of the eardrum	10
(b) Schematic outline of the eardrum	10
Fig. 2.4 The middle-ear ossicles, their ligaments and muscles	13
Fig. 3.1 Average transformation of sound pressure from free field to human eardrum as a function of frequency at eight values of angle of incident sound	17
Fig. 3.2 Average acoustic pressure gain for various ear components	18
Fig. 3.3 Standing-wave ratios derived from various investigations	20
Fig. 3.4 Holographic image of cat eardrum vibration	26
Fig. 3.5 Eardrum vibration patterns determined by the finite-element method for the first six natural frequencies	29
Fig. 3.6 Schematic block diagram of the human middle ear	32
Fig. 3.7 Circuit diagram of the human middle ear	33
Fig. 3.8 Ratio of plane-wave radiation coefficient to the sum of radiation coefficients for all higher modes and percentage of acoustic coupling of model cat eardrums attributable to nonplanar modes	37
Fig. 3.9 Standing pressure waves in the ear canal	
(a) Amplitude of modes at 1 kHz	38
(b) Amplitude of modes at 15 kHz	38
Fig. 4.1 Some typical element types	41
Fig. 4.2 Natural coordinates for the quadrilateral	48
Fig. 4.3 Quadrilateral area determination	63
Fig. 5.1 Finite-element meshes for the eardrum and ear canal	74

Fig. 5.2 Eigenvalue analysis of the eardrum (circular plate): First six modes	76
Fig. 5.3 Eigenvalue analysis of the ear canal (cylindrical tube): First six modes	80
Fig. 5.4 Results for the coupled problem at 100 Hz	
(a) Eardrum: real component	85
(b) Eardrum: imaginary component	85
(c) Ear canal: real component	86
(d) Ear canal: imaginary component	86
Fig. 5.5 Results for the coupled problem at 3.5 kHz	
(a) Eardrum: real component	87
(b) Eardrum: imaginary component	87
(c) Ear canal: real component	88
(d) Ear canal: imaginary component	88
Fig. 5.6 Results for the coupled problem at 7.1 kHz	
(a) Eardrum: real component	89
(b) Eardrum: imaginary component	89
(c) Ear canal: real component	90
(d) Ear canal: imaginary component	90

LIST OF TABLES

Table 1.1 Human ear-canal variation	8
Table 5.1 Finite-element and theoretical frequencies for the first six modes of the eardrum	77
Table 5.2 Finite-element and theoretical frequencies for the first five longitudinal modes of the ear canal	79
Table 5.3 Finite-element and theoretical frequency for the first transverse mode of the ear canal	81

PRINCIPAL NOTATION

A	area of two-dimensional region
B	strain-displacement matrix
C	constitutive or elasticity matrix
D	damping matrix
E	modulus of elasticity
f	frequency
F	force vector
G	modulus of rigidity
H	vector of shape functions
J	Jacobian operator
K	stiffness matrix
M	mass matrix
P	acoustic pressure
U	displacement vector
U	strain energy
V	potential energy
δ	variational operator
γ	shear strain vector
ϵ	normal strain vector
ν	Poisson's ratio
Π	functional of the problem

σ	normal stress vector
ρ	mass density
τ	shear stress vector
ω	angular frequency

CHAPTER 1

INTRODUCTION

In this study, mathematical modelling methods are developed for examining the interaction between the acoustical behaviour of the ear canal and the mechanical behaviour of the eardrum in humans. A greater knowledge of how sound-pressure distributions in the ear canal interact with the eardrum is essential in order to have a better quantitative understanding of how sound energy is transmitted to the middle ear. In an experimental context, the kind of understanding acquired from such a study would allow the proper interpretation of various physiological acoustic experiments. In a clinical context, the greater understanding would allow the extraction of more information from non-invasive diagnostic tests. Ultimately, knowledge obtained from examining ear canal and eardrum interactions is relevant to the design of hearing-aids and earphones.

Modelling the coupled system of the ear canal and the eardrum is not a simple matter. Because the pressures at the end of the ear canal influence the mechanical motion of the eardrum and vice versa, modelling should involve some sort of feedback technique. Ear canal/eardrum modelling is an example of a problem involving fluid-structure interaction. Analytical solutions to these fluid-structure problems are usually limited to simple geometries. Numerical methods such as finite-element analysis must be used when the system becomes more complex. In recent years there has been considerable interest in applying finite-element computer programs to the solution of fluid-structure interaction problems. Finite-element analysis involving fluid-structure interaction has been applied to diverse systems including nuclear reactor components, naval and aerospace structures, dam/reservoir systems, and vehicle passenger compartments, as well as biological systems (Akkas et al., 1979).

The work presented here deals with an initial attempt at modelling ear canal and eardrum interaction using the finite-element method. To begin, an overview of the anatomy and physiology of hearing is presented in Chapter 2. Chapter 3 presents a review of relevant research in the study of the acoustical behaviour of the ear canal, and the mechanical behaviour of the eardrum and middle ear. Various approaches to modelling the ear canal, eardrum and middle ear are also overviewed, as well as work which has actually examined the problem of ear canal/eardrum interaction. An introduction to the concepts of finite-element modelling is given in Chapter 4, as well as explanations on how the finite-element code is altered to deal with, first, the acoustic modelling in the ear canal, and second, the actual implementation of the interaction problem. The actual models used for the ear canal and eardrum, and results obtained for both the uncoupled and coupled problems, are presented in Chapter 5. As there remains a good deal of work to be done before the complete aims of this project are realized, Chapter 6 discusses the future directions which this work will take, as well as other conclusions.

CHAPTER 2

PHYSIOLOGY OF THE EXTERNAL AND MIDDLE EAR

2.1 INTRODUCTION TO THE HEARING SYSTEM

The human ear (Fig. 2.1) is a complex and sensitive organ which is divided into three main parts: the outer, middle and inner ear. The ear canal collects sound and leads it inward to the tympanic membrane which separates the outer ear from the middle-ear cavity. The air-filled middle-ear cavity contains three bones or ossicles : the malleus (hammer), the incus (anvil) and the stapes (stirrup), together with supporting ligaments and muscles. Sound is transmitted from the tympanic membrane to the malleus, from the malleus to the incus, and from the incus to the stapes, which covers the oval window, and thus to the liquid-filled inner ear. The middle ear acts as an impedance-matching device: it transforms acoustic sound pressure in front of the tympanic membrane into fluid pressure within the inner ear. The ossicular chain amplifies the sound pressure it conveys: first, by a mechanical lever action; and second, by pressure amplification due to the fact that the area of the oval window is about seventeen times smaller than that of the tympanic membrane. Therefore the total pressure gain in the middle ear insures effective sound transfer to the fluid-filled inner ear. The inner ear contains the cochlea, a tube approximately circular in cross-section and wound in the shape of a spiral shell. It is here that the mechanical energy is converted to neural activity in the production of frequency-coded signals. The final step in hearing occurs when these coded signals from the cochlea are interpreted in the auditory centres of the brain.

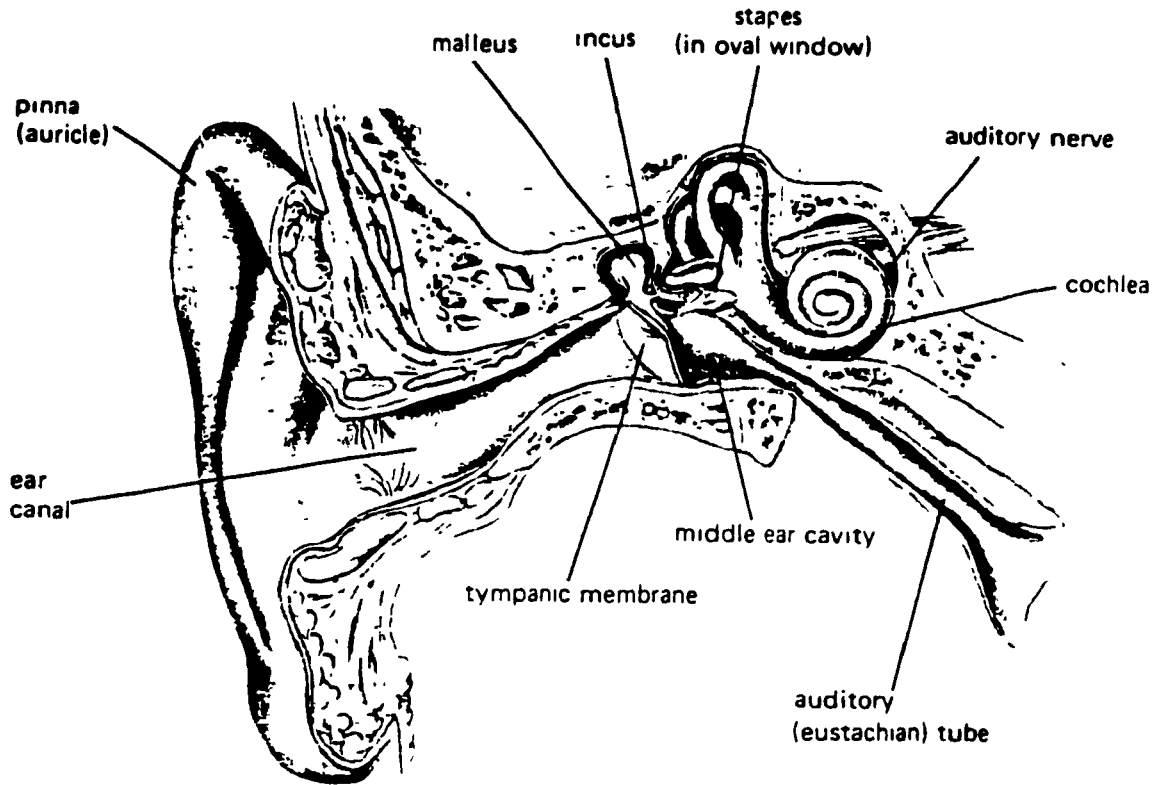


Fig. 2.1

The human ear. From Vander et al. (1985, p. 659).

2.2 THE EXTERNAL EAR

2.2.1 THE PINNA

The outer ear is composed of two components: the pinna or auricle of the external ear, which is the "visible flap" of the ear; and the ear canal, or external auditory meatus. The pinna consists of a thin plate of cartilage covered with skin. It may be subdivided into the concha, the cavity which surrounds the entrance to the ear canal; the helix, which is the rim of the pinna; and the lobule, the soft lower end of the pinna. A diagram of the pinna and its associated features can be found in Fig. 2.2. According to Shaw (1980), certain individual structures are of special interest at high frequencies: the fossa, which is acoustically connected to the cymba, and the crus helias, which separates the cymba from the cavum. Other structures including the helix, the antihelix and the pinna extension or lobule apparently function together as a simple flange (Shaw, 1975).

The human pinna flange is small relative to head size and is therefore not a very efficient sound collector. The pinna flange's primary function seems to be in sound localization. Roffler and Butler (1968) and Gardner and Gardner (1973) have respectively shown that if human pinna activity is impeded, or if the pinna is progressively occluded, localization of sound is hindered.

Average measurements for the human concha indicate a depth of 13 mm, a volume of 4500 mm³ and a radius of 8.9 mm (Wever and Lawrence, 1954). The concha acts as a cavity resonator producing a pressure increase of about 10 dB at approximately 5 kHz (Teranishi and Shaw, 1968).

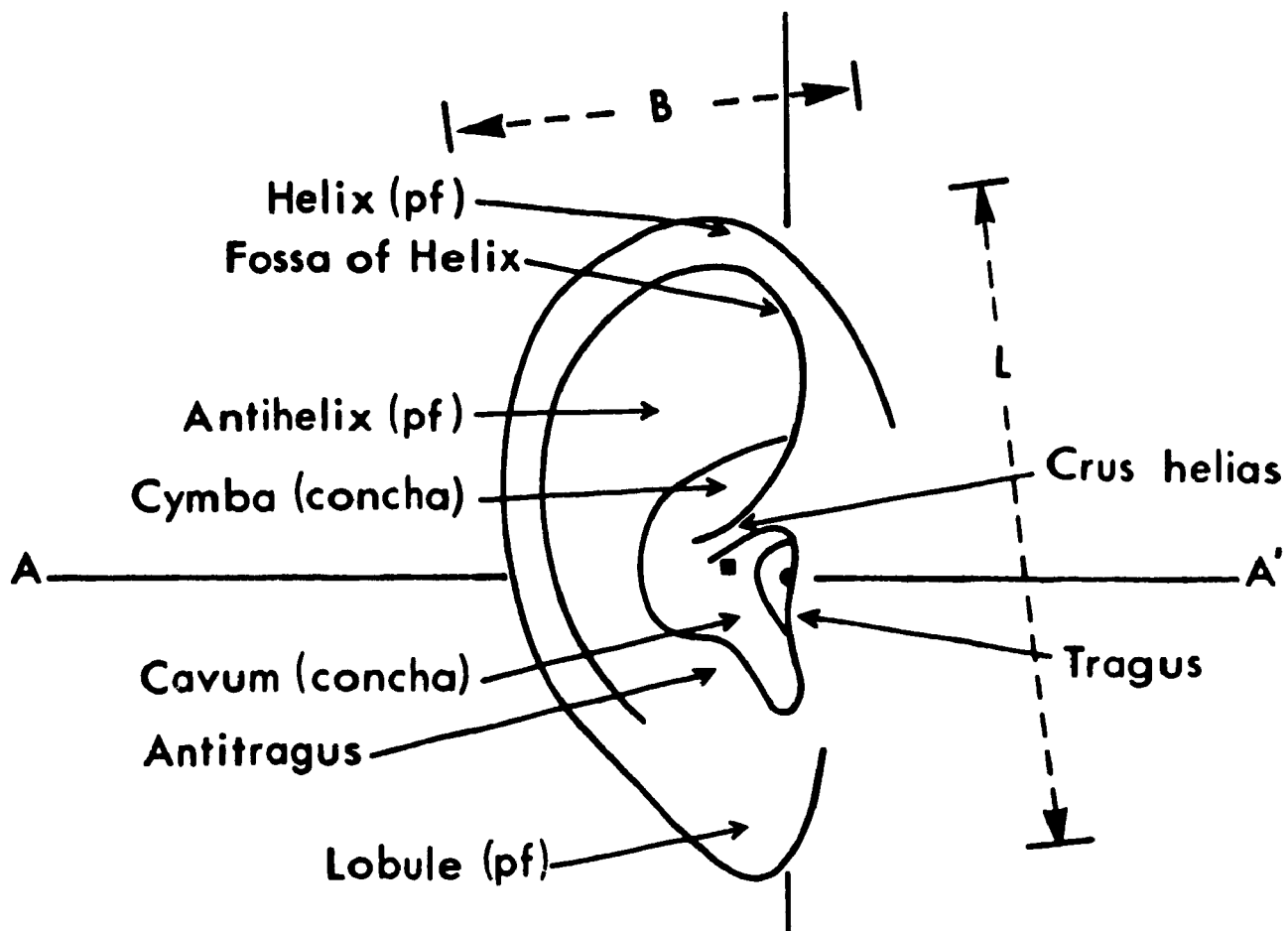


Fig. 2.2

View of the external ear. From Shaw (1974, p. 456).

The pinna varies greatly amongst different species. For example, cat and guinea-pig pinnae differ in shape from those of the human and are much larger in proportion to the size of the head. Also, it is not clear whether cat and guinea-pig pinnae have subdivisions of concha, helix and lobule corresponding to those in the human ear. Furthermore, cats, unlike humans, are able to turn their pinnae towards a sound source without moving the head.

2.2.2 THE EAR CANAL

Refer again to Fig. 2.1 for an illustration of the human ear canal. Interesting aspects of the geometry include a sharp bend upward and to the rear near the entrance of the canal and a downward curve by the eardrum. Wever and Lawrence (1954) and Johansen (1975) determined that the human ear canal has a mean length of about 25 mm. Wever and Lawrence give the ear canal a mean diameter of about 7mm and a volume of approximately 1000 mm³. More recently, Stinson and Lawton (1989) studied human ear-canal geometry giving an idea of the range of variation among humans. Results obtained for range and mean value of ear-canal length, volume and cross-sectional area from fifteen cadaver moulds are given in Table 1.1. The angle between the base of the eardrum cone and a section normal to the ear canal close to the eardrum has been found to be about 70° (Johansen, 1975).

	<i>Length</i> (mm)	<i>Volume</i> (mm ³)	<i>Average Area</i> (mm ²)
<i>Range</i>	27-37	910-1725	30.0-54.9
<i>Mean</i>	30.8	1271.3	41.9

Table 1.1 Human ear-canal variation (calculated from Stinson and Lawton data, 1989).

The ear canal is greatly variable among different species. The cat ear canal is quite different from that of the human. A cylindrical portion extends out from the eardrum for about 15 mm. The ear canal then bends sharply at a right angle and the cross-sectional area becomes narrower and dumbbell-shaped and leads to the pinna (Wiener et al., 1965). The cat ear canal has a length of about 20 mm. The guinea-pig ear canal is shaped like a tube about 10 mm in length and 2.5 mm in diameter, although at the end of the canal it expands sharply to approximately 8 mm, the diameter of the eardrum (Sinyor, 1971; Sinyor and Laszlo, 1973).

Mechanical Properties of the Ear Canal

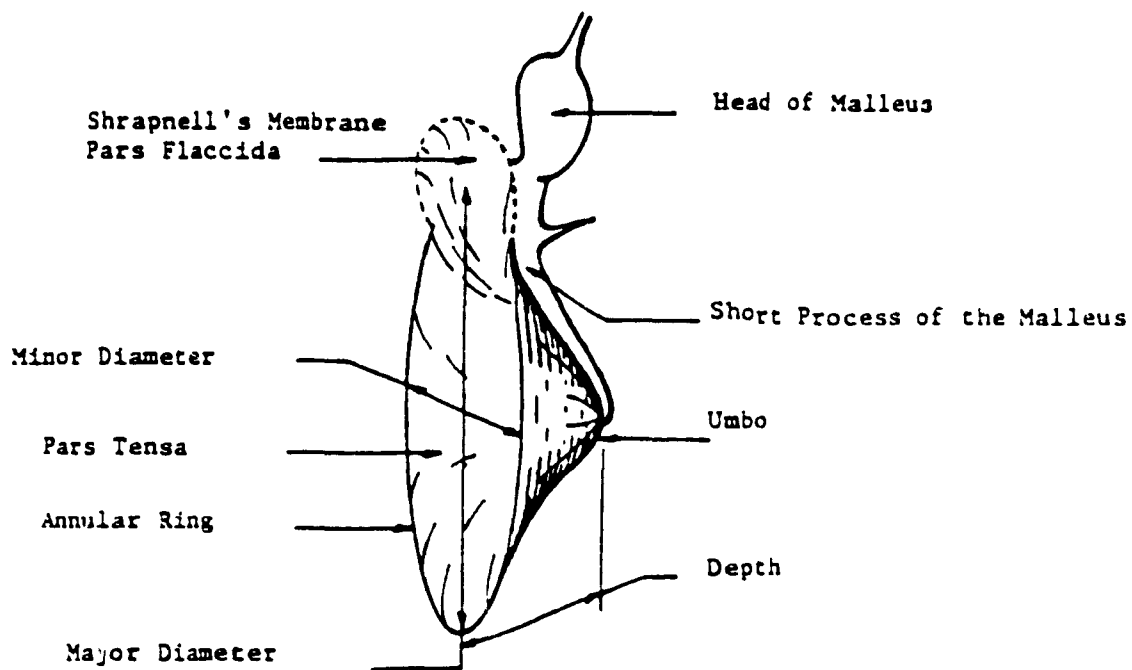
The ear canal is lined with an epidermal layer. In the human ear, the epidermal layer is backed by bone near the eardrum and cartilage in the rest of the canal. Based on estimates of elastic moduli for epidermis, cartilage and bone from Fung (1981), the ear canal has a dilatational

impedance that is 10^4 times larger than that of air (Rabbitt and Holmes, 1988). Thus the ear-canal wall can be treated as rigid.

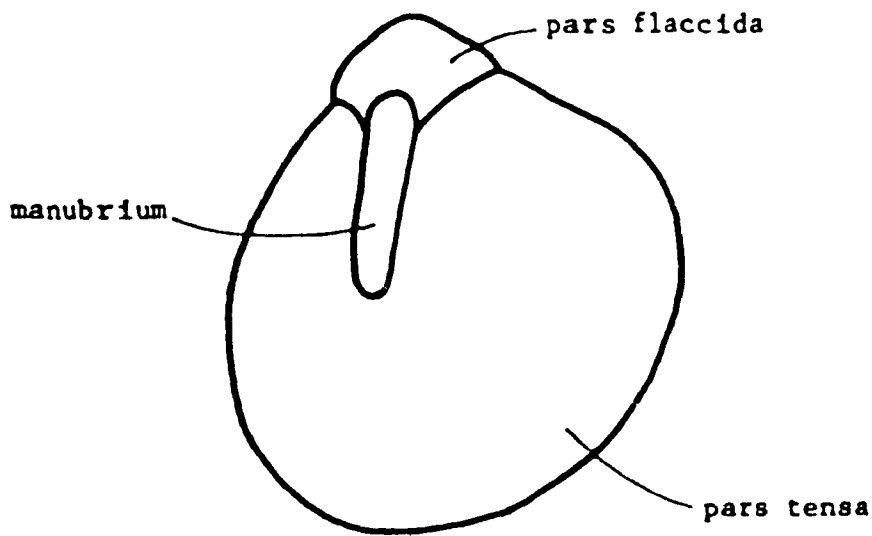
2.3 THE EARDRUM

A diagram and schematic outline of the human eardrum are given in Fig. 2.3. The eardrum is conical in shape with its apex pointing medially. The sides of the cone are convex outward. Referring to the schematic outline of the eardrum, there are three distinguishable areas: the *pars tensa*, the *pars flaccida* and the *manubrium*. The bony process of the malleus, known as the *manubrium*, attaches to the eardrum near the *umbo*, the point of deepest concavity of the eardrum. The *pars tensa* forms the main surface of the eardrum and is composed of three layers of tissue: an outer epidermal layer; the *lamina propria*, consisting of two connective tissue layers and a fibrous layer; and an inner mucosal layer. The fibrous layer of the *lamina propria* forms the main structural component of the eardrum. It is composed of fibres that are circularly and radially arranged. The *pars tensa* is anchored to the bone around most of its circumference by the *annular ligament*. The *pars flaccida* is superior to the *manubrium*. It is the more elastic part of the eardrum and is separated from the *pars tensa* by the *annular ligament*. The major diameter of the human eardrum ranges from 9 to 10.2 mm and the minor diameter ranges from 8.5 to 9.0 mm (Rabbitt, 1985). The eardrum varies in thickness from 30 to 90 μm (Lim, 1970).

In terms of inter-species variation, the size of the eardrum tends to vary less among species than overall body size. Khanna and Tonndorf (1969) found among seven different



(a)



(b)

Fig. 2.3

The human eardrum.

(a) Sketch of the eardrum. From Rabbitt (1985, p.25).

(b) Schematic outline of the eardrum. After Kojo (1954).

mammals that the area of the tympanic membrane is approximately proportional to a linear dimension of the whole body, such as the cube root of weight.

Mechanical Properties of the Eardrum

Békésy (1949) measured the bending stiffness of human cadaver eardrums and determined it to be $2 \times 10^7 \text{ N/m}^2$. Kirkae (1960) determined values two or three times stiffer than Békésy. Decraemer (1980) obtained results in good agreement with Békésy.

There are no data available concerning the Poisson's ratio of the eardrum. It appears that the value has little effect (Funnell, 1975). Funnell and Laszlo (1982) point out that for a material composed of parallel fibres with no lateral interaction among fibres, the Poisson's ratio would be zero for stress applied in the direction of the fibres. Common materials have a Poisson's ratio ranging from 0.3 to 0.5. Funnell and Laszlo (1978) use a value of 0.3 for their eardrum model.

The eardrum presumably has a volume density somewhere between that of water (1000 kg/m^3) and that of undehydrated collagen (1200 kg/m^3) (Harkness, 1961).

2.4 THE MIDDLE EAR

The human middle ear contains several interconnected air-filled chambers: the main chamber or tympanic cavity which lies behind the eardrum; a smaller cavity, the epitympanum which lies above and extends backward and laterally; and small cavities called pneumatic cells, which line the upper part of the middle ear. The malleus, the incus and the stapes are suspended within the middle-ear cavities by a set of ligaments and by the tensor tympani and stapedius

muscles (Fig. 2.4). The malleus is supported by anterior, lateral and superior ligaments. The incus is supported by a posterior ligament. At low frequencies, the middle-ear axis of rotation lies approximately between the line joining the posterior incudal ligament and the anterior malleolar ligament. The annular ligament (not to be confused with the annular ligament of the eardrum) connects the footplate of the stapes to the oval window. Finally, a ligament also exists between the malleus and the drum membrane. The tensor tympani muscle is attached to the malleus and when it contracts it pulls the malleus and therefore the eardrum further into the middle ear. The stapedius muscle is connected to the stapes and pulls it sideways during contraction.

The cat and guinea-pig middle ears are similar in overall anatomical structure and function to that of man, although there are various differences in detail (Funnell, 1975).

Mechanical Properties of the Middle Ear

Ligaments and muscles are composed of connective tissue made up of fibres which contain collagen, elastin and other proteins. The problem in modelling the muscles and ligaments is more than a non-linear elastic problem, because the response of tissues is loading-path and rate dependent. Some preliminary finite-element modelling of cat middle-ear ligaments by Funnell (1989), has assumed material and geometric linearity, as well as isotropic and homogeneous materials. It is possible, however, to use the finite-element method to solve problems characterized by nonlinearities, inhomogeneities and anisotropy

AUDITORY OSSICLES - Ligaments and Muscles

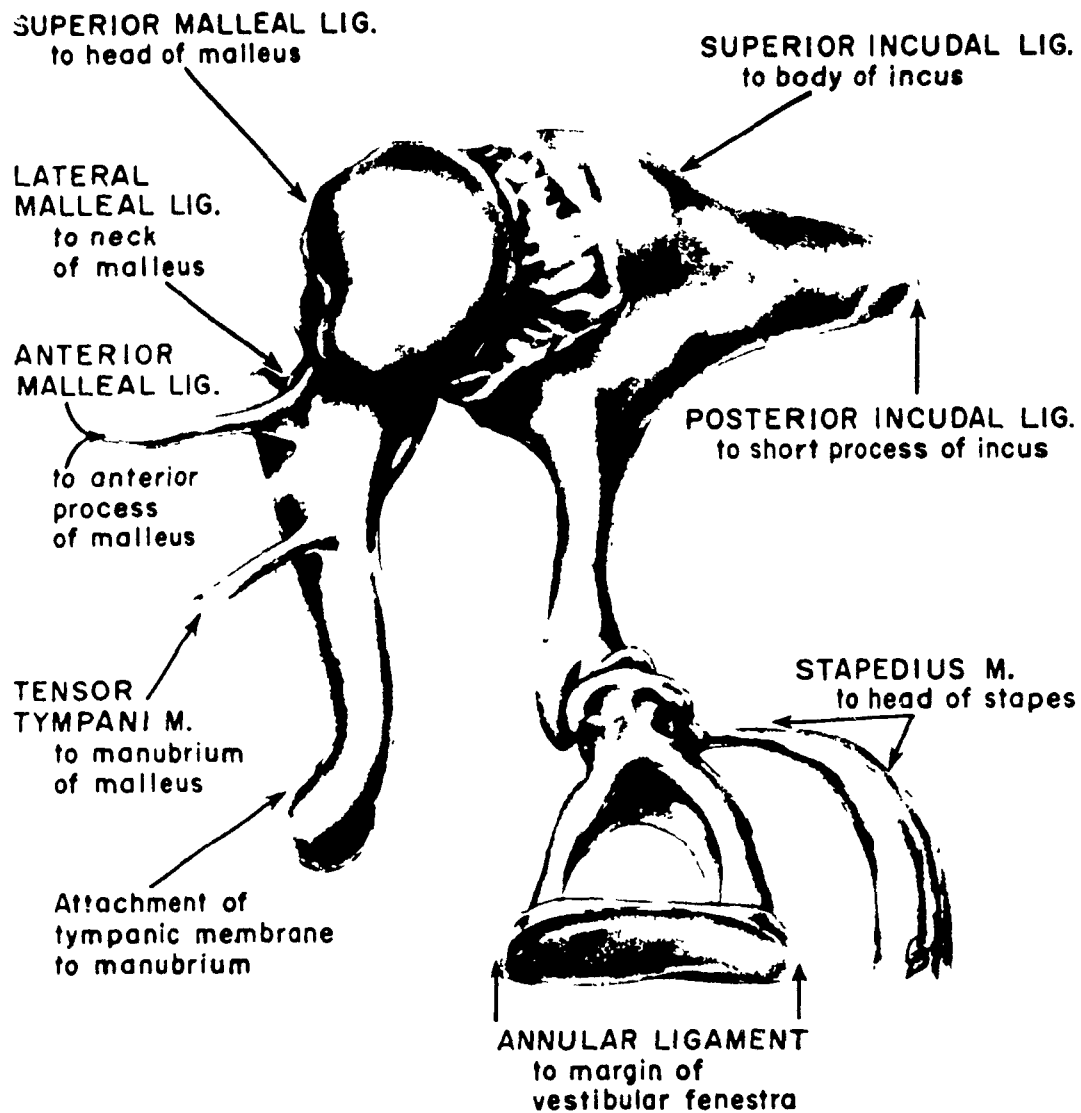


Fig. 2.4

The middle-ear ossicles, their ligaments and muscles.
From Anson and Donaldson (1973, p. 245).

The middle-ear ossicles are generally modelled as rigid. However, Decraemer et al. (1989) found some evidence of bending of the manubrium. The matter may therefore need further consideration.

CHAPTER 3

EXPERIMENTAL OBSERVATIONS AND MODELLING OF THE EXTERNAL AND MIDDLE EAR

3.1 INTRODUCTION

This chapter presents a historical review of literature concerning experimental observations on the ear canal, eardrum and middle ear. Various approaches to modelling the outer and middle ear are also discussed. First, a summary of ear canal work is presented; followed by a coverage of eardrum and middle-ear studies; concluding with a discussion of the initial attempts made to deal with the coupled problem.

3.2 THE EAR CANAL

3.2.1 SOUND-PRESSURE EXPERIMENTS IN THE EXTERNAL EAR

Some of the earliest research that examined pressure distributions in the ear canal includes the well-known work of Weiner and Ross (1946). Weiner and Ross inserted a microphone along the auditory canal of human subjects. A plane progressive wave from a loudspeaker served as a free sound field for the subject. A sound pressure increase of 12 dB was found at the eardrum with a peak around 3 kHz. If one considers the ear canal as a cylindrical cavity open at one end and closed at the other, this peak is effectively due to the fundamental longitudinal resonance of

the ear canal. Besides this first resonance at $\lambda/4$, other modes at $3\lambda/4$ and $5\lambda/4$ interact with concha modes at higher frequencies to increase the number of resonances. Weiner and Ross used incident angles of 0, 45 and 90 degrees for the incident waves.

Other early external ear studies include the work of Shaw and Teranishi. Shaw and Teranishi (1968) performed experiments on real ears and rubber replicas. The rubber model replicated the dimensions of the human pinna, concha and ear canal. A point source at various angles of incidence from 1 to 15 kHz was used. Sound pressure was measured with a probe tube microphone at certain positions with the ear canal open and blocked. The replica data were in agreement with real ear data for frequencies up to 7 kHz. In conjunction with this work, Teranishi and Shaw (1968) constructed physical models with simple geometry. A cylindrical cavity was set in an infinite plane to represent the concha. The pinna was modelled by a rectangular flange attached to the inclined concha and the cylindrical canal was completed with a 2-element network representing the eardrum impedance. The simple model was in good agreement with real ear data for frequencies up to 7 kHz.

Many researchers have undertaken basic ear-canal pressure studies. Shaw (1974) synthesized data from 10 studies and 5 different countries for various angles of incidence. The synthesized data are displayed in Fig. 3.1, from Shaw (1974), indicating the average sound-pressure transformation from free field to eardrum for frequencies from 0.2 to 12 kHz. Shaw (1974) also summarized the various contributions of the components of the external ear as well as the head, neck and torso to the acoustic pressure gain (see Fig. 3.2). At frequencies less than 350 Hz, the head has no effect. It adds about 5 dB when the frequency is raised to 10 kHz. The torso can have different effects depending on the frequency range considered. It has an amplifying effect at low frequencies, an attenuating effect around 1.5 kHz, and no effect at higher frequencies. The pinna flange produces a 3 dB increase around 4 kHz.

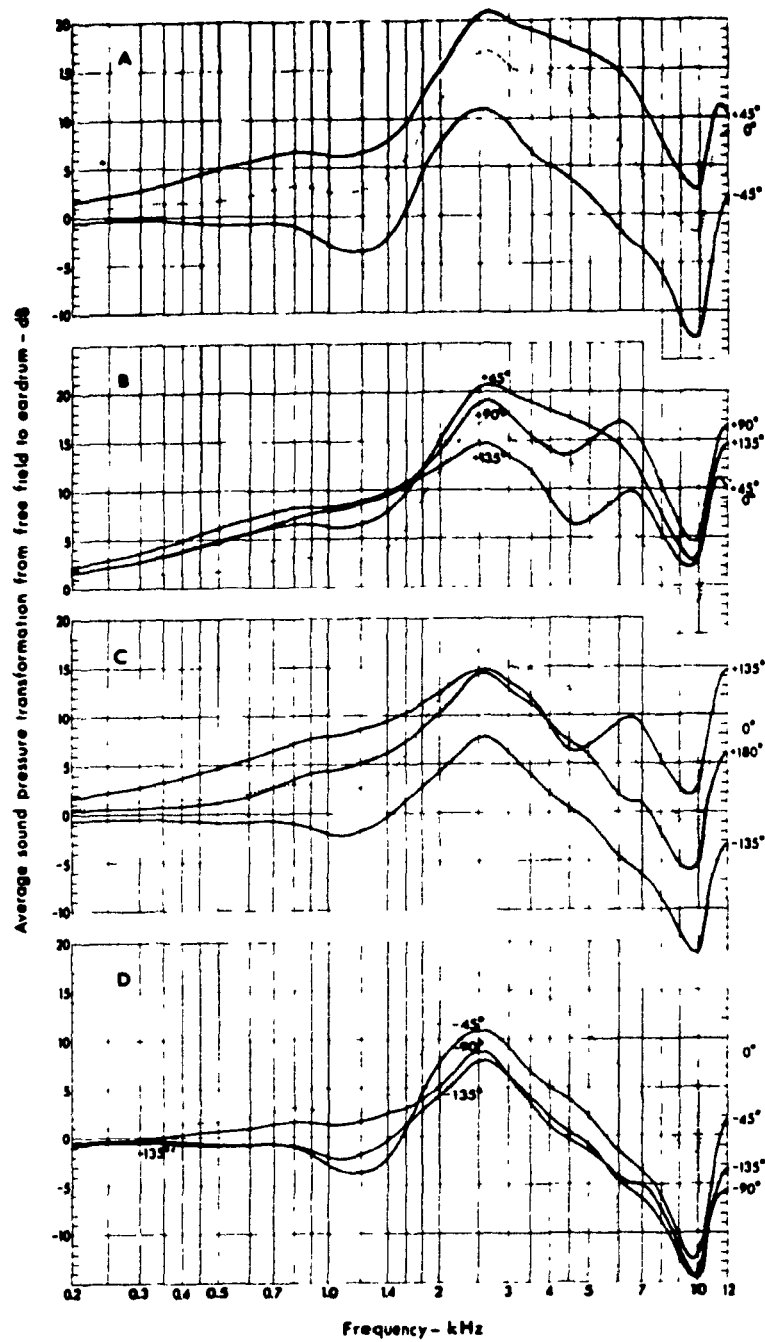


Fig. 3.1

Average transformation of sound pressure from free field to human eardrum as a function of frequency at eight values of angle of incident sound. From Shaw (1974).

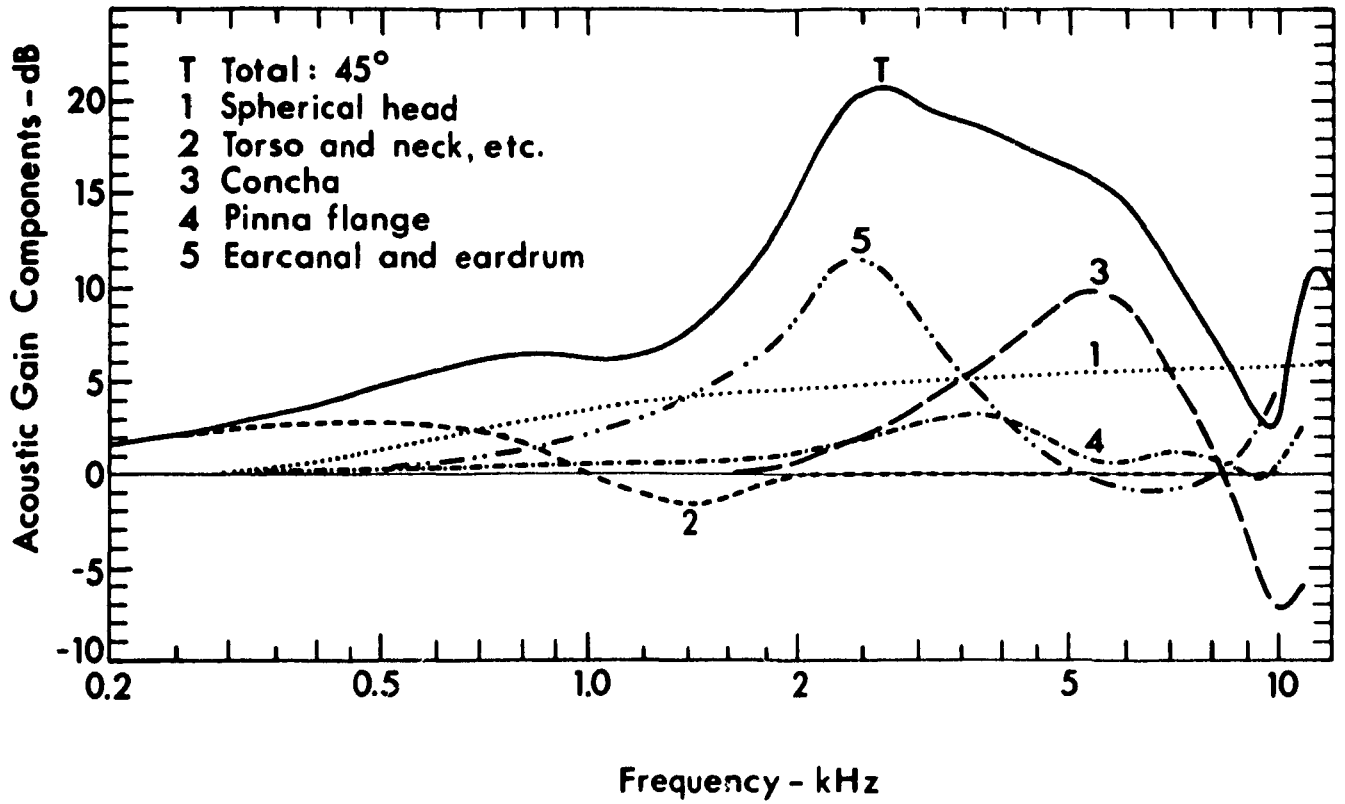


Fig. 3.2

Average acoustic pressure gain for various ear components. (Incident sound at an angle of 45°.)
From Shaw (1974, p. 468).

3.2.2 ENERGY REFLECTANCE STUDIES

Some research in recent years has focused on the determination of the coefficient of reflection of acoustic energy at the eardrum. Energy reflectance is relatively insensitive to anatomical geometry at higher frequencies, as opposed to the method of eardrum impedance which becomes an unreliable method to determine input to the middle ear at such frequencies due to difficulties in differentiating between eardrum impedance and the effects of ear-canal geometry.

Stinson, Shaw, and Lawton (1982) studied standing wave ratios in the ear canal. A significant portion of the acoustic energy entering the ear canal is reflected back along the canal from the eardrum. Standing waves result because of the interference between incident and reflected waves. Standing wave ratios were determined for a range of 5 to 10 kHz by examining the sound field set up in occluded human ear canals. The standard impedance tube method was employed; that is, assuming a uniform duct terminated by an acoustic load, the sound pressure is measured as a function of position, and pressure maxima and minima are used to calculate the energy reflection coefficients. Over the 5 to 10 kHz range, energy reflectance values of 60-78% were obtained; these values were considerably higher than those determined from previous studies. Fig. 3.3 compares experimental values of standing wave ratios determined in various studies. Lawton and Stinson (1986) also used standing wave patterns to estimate acoustic energy reflectance. Standing wave patterns were measured in unoccluded ear canals of human subjects for pure tones ranging from 3 to 13 kHz. The region where probe measurements were made was assumed to be a duct of constant cross-section. The energy coefficient was found to rise from 0.3 at 4 kHz up to 0.8 at 8 kHz, staying at this value up to 13 kHz. These data agreed well with those of Stinson et al. (1982).

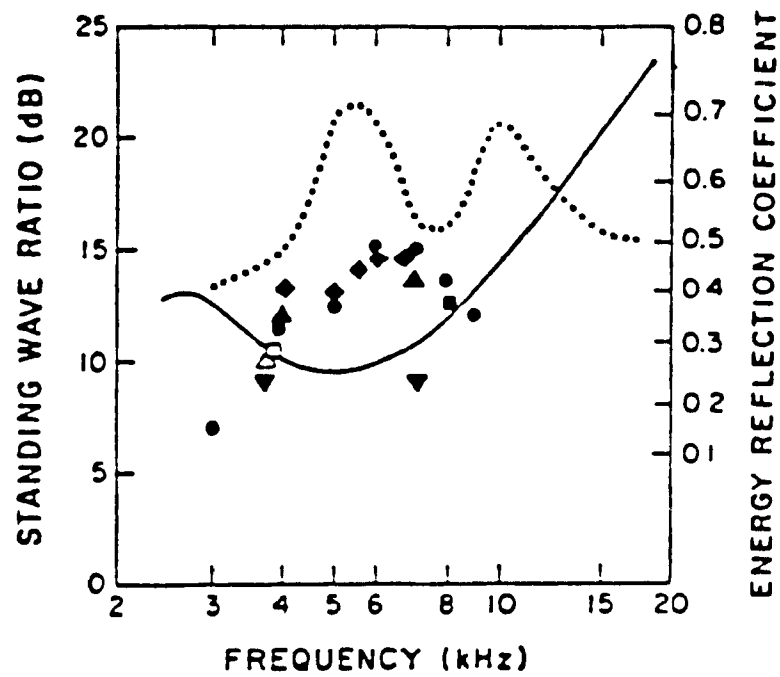


Fig. 3.3

Standing wave ratios derived from various investigations. On the right, the vertical axis shows the corresponding energy reflection coefficient. The symbols, dotted line and solid curve indicate the different authors of the investigations. From Stinson et al. (1982, p 768).

Stinson (1985a) determined acoustic reflection coefficients at a duct termination by measuring the maximum rate change of phase with position. The method produced results similar to the usual impedance tube method where amplitude components are considered. The advantage of this phase method is that only a small amount of space is required to make the measurements; this avoids potential injury associated with increasing the penetration of the probe. The method is valid for ducts with uniform cross-section as well as for ducts with conical area functions, but otherwise it is still restricted.

Rabbitt (1988) used a high-frequency asymptotic theory (refer to Rabbitt and Holmes, 1988, in Section 3.4) combined with multiple sound-pressure measurements in the ear canal to determine energy flow and planar standing wave equations. The theory agrees well with experimental measurements in replicas of human ear canals from Stinson (1985b), but is limited to high frequencies and is not valid at the terminating end of the canal. (Multidimensional effects are not included; only the plane wave component of the pressure field is dealt with.)

3.2.3 NETWORK MODELLING OF THE EAR CANAL

External ear modelling has sometimes involved the network representation of the ear canal. Zwislocki, whose influential work in middle-ear acoustics (1962) involved the development of electrical analogs (refer to Section 3.4.2), also used electrical networks to calculate theoretical sound pressure in the ear canal (1965). Inductance and capacitance are made analogous to acoustic mass and compliance. To form a network model, inductive and capacitive Tee sections are connected in series, with the number of sections depending on the high frequency limit (Bauer, 1965). Zwislocki's model agreed well with data obtained by Weiner and

Ross (1946). Further work in this area was undertaken by Gardner and Hawley (1972). The ear canal was represented by a 10-section analog network of uniform and tapered design. Two-branch and four-branch networks for the representation of the eardrum and adjacent structures were found effective. Using values from Zwislocki (1970) of canal length equal to 22.5 mm and canal radius equal to 3.74 mm, values of inductance and capacitance were calculated from standard uniform tube formulas.

3.2.4 STUDIES FOCUSING ON EAR-CANAL GEOMETRY

Although there has been some interest in network modelling, the uniform tube has been the most popular model approximation to the real ear canal. At low frequencies, wavelengths are much larger than ear-canal dimensions, so that the cylindrical tube model is a reasonable approximation for the geometry of the ear canal. However, at high frequencies where variations over small distances are significant, this approximation no longer holds. Therefore, certain recent research has focused on the importance of the actual shape of the ear canal in determining acoustic input to the middle ear, and thus the limited validity of the cylindrical ear-canal model.

Stinson and Shaw (1982), using experimental cavities of different shapes and a simulated eardrum, determined that the geometry of the eardrum and adjoining section of ear canal affect the flow of energy to the middle ear. Hudde (1983) measured sound pressure at three locations to determine the area function of the human ear canal. The area function is the variation of the cross-section along the middle axis of the duct. As areas were obtained for cross-sections at right angles to a straight axis, curvature was not taken into account. Stinson and Shaw (1983) determined the importance of geometry at frequencies greater than 10 kHz. The sound-pressure distribution was measured in a scaled replica of the ear canal, and a theory was developed to

express the ear canal in terms of cross-sectional areas defined along a curved axis using an extension of Webster's one-dimensional horn equation. The first paper to present the mathematics of this theory was that of Khanna and Stinson (1985). The modified horn equation is applied to three-dimensional, rigid-walled tubes that have variable cross-section and curvature along their length. The equation is expressed as:

$$\frac{d}{ds} \left(A(s) \frac{dp_o(s)}{ds} \right) + k^2 A(s) p_o(s) = 0 \quad (3.1)$$

where s represents the curved axis, $A(s)$ are the area functions, perpendicular to the s axis, k is the wave number, and p_o is the pressure along the axis. The total solution $p(s)$ can be considered as the sum of two linearly independent solutions, propagating in the $+s$ and $-s$ directions. Numerical techniques are used to determine the s axis, and $A(s)$ is determined from silastic casts of the ear canal. Khanna and Stinson also measured sound pressure between 100 Hz and 33 kHz at 14 different locations in the ear canal of a cat. Large variations of sound pressure were observed along the ear canal and over the surface of the eardrum above 10 kHz. The shapes of the standing wave patterns agreed well with results obtained from using the theoretical horn equation approach for frequencies above 12 kHz. However, the analysis assumed rigid walls, so that if high-frequency absorption should occur, modifications in theory would need to be made. This modification was undertaken by Stinson (1985b). Stinson measured sound pressure distributions in scaled replicas of human ear canals. Using the horn extension theory, absorption of acoustic energy at the eardrum was accommodated by incorporating an effective eardrum impedance acting at a single point. Theory agreed well with measurements, and at frequencies greater than 6 kHz it was clear that the theory was an improvement over that of the uniform tube.

Rabbitt (1988) determined ear-canal cross-sectional area functions using the asymptotic theory in conjunction with pressure measurements. Because only two frequencies were used, the calculated area functions do not take full advantage of the theory. Future applications of the theory over a broader frequency spectrum are expected to improve results.

Stinson and Lawton (1989) studied the geometry of 15 ear canals by making rubber moulds, and by using a mechanical probe system to record 1000 coordinate points over the surface of the mould. Ear canals were described with respect to a curved axis. Area functions were then derived, which were in agreement with work done by Johansen (1975) and Hudde (1983). Large inter-subject variations were found. Area functions were used in conjunction with the one-dimensional horn equation to predict sound-pressure distributions in human ear canals up to 19 kHz. Variations in ear-canal geometry produced the greatest sound pressure transformation from the canal entrance to the innermost region for frequencies greater than 10 kHz. Therefore, the accurate specification of ear-canal geometry is important in the proper prediction of sound-pressure distribution.

3.3 THE EARDRUM

3.3.1 EXPERIMENTAL OBSERVATION OF EARDRUM VIBRATIONS

There has been a great deal of research undertaken involving experimental observations of eardrum function as well as theoretical modelling of eardrum behaviour. For a historical review the reader is referred to Funnell & Laszlo (1982). Most observations of eardrum vibrations have been at low frequencies — from 1 to 2 kHz. Kessel (1874) performed some of

the earliest research on eardrum vibrations. Displacements of human cadaver eardrums due to static pressures were observed using a magnifying lens. Kessel also used a stroboscope to observe vibrations at 256 and 512 Hz. The greatest displacements were seen in the posterior section of the eardrum. Mader (1900) employed a mechano-electrical probe to study human cadaver eardrum vibrations using 240 Hz and 600 Hz tones. The greatest amplitudes occurred in the posterior/inferior quadrant of the drum. Dahmann (1929, 1930) used mirrors to observe the displacements on human cadaver eardrums. Using a static pressure change of 170 dB SPL, it was determined that the middle parts of the drum undergo larger displacements than the manubrium. In this study only one illustration was published — a sketch of the eardrum with marks superimposed representing the loci of reflected beams of light from the mirrors. Capacitive probe measurements on human cadavers were made by Békésy in 1941. Again, only one illustration was published. Sound pressures and displacements were not presented. Békésy concluded that the eardrum (except for the extreme periphery) and the manubrium vibrate as a stiff surface. Stroboscopic methods were used by Kobrak (1941) for cadavers and living subjects, but no results were presented in the discussion. Perlman (1945) also used stroboscopic methods and reported that the amplitude of vibration on the anterior and posterior regions was about the same in cadaver eardrums. The first high-resolution work using holographic methods was undertaken by Khanna (1970). In a frequency range covering 400 Hz to 6 kHz, complete iso-amplitude contour maps were produced. Holographic methods were used on live cats (Khanna and Tonndorf, 1972) and on human cadavers (Tonndorf and Khanna, 1972). The displacements on the manubrium were smaller than those of the surrounding membrane, and the largest displacements were found in the posterior segment. An example of eardrum output from Khanna and Tonndorf (1972) is given in Fig. 3.4.

At low frequencies the general conclusion made by most of these experiments was that the displacements of the manubrium are less than those of the surrounding membrane. The main conflicting view comes from Békésy who concluded that the eardrum vibrated as a stiff plate, but subsequent work has effectively invalidated this notion.

High frequency response of the eardrum has been examined by a few researchers. In their holographic study, Khanna and Tonndorf (1972) observed cat eardrum vibrations up to 6 kHz. The low-frequency pattern was present at 2.5 kHz but broke up as the frequency increased. Similar results were found for human ears (Tonndorf and Khanna, 1972). More recently, Decraemer, Khanna, and Funnell (1989) examined the amplitude and phase of eardrum and malleus vibrations up to approximately 20 kHz in anaesthetized cats. Up to 10 kHz, results obtained were similar to those of Khanna and Tonndorf (1972), including a low-frequency plateau up to about 3 kHz and minima around 4 kHz. Above 5 kHz, resonances were present. Between 10 and 20 kHz, the vibration amplitude was found to oscillate around a value about 20 dB lower than the low-frequency plateau level. Different points on the eardrum were found to vibrate in phase at frequencies below 1 kHz. At higher frequencies, points vibrated out of phase.

3.3.2 THEORIES AND MODELS OF EARDRUM BEHAVIOUR

Lumped-parameter models of the eardrum are popular, especially in connection with lumped-parameter middle-ear modelling in general (refer to Section 3.4.2). In a lumped-parameter model, certain characteristics of a system are lumped into distinct circuit elements, thus producing an equivalent circuit (which could be electrical, mechanical or acoustical). Generally the parameters are not closely tied to actual physical or anatomical data, but these models are appealing due to their simplicity. Shaw (1977) and Shaw and Stinson (1981) used a 2-piston

lumped-parameter model for the eardrum, where one piston or zone represented the vibrating portion of the eardrum, and the other represented the eardrum/malleus coupling. In 1986, Shaw and Stinson extended work to a three-zone model where the free vibrating zone was divided into anterior and posterior zones.

Early attempts to account for shape in eardrum models, for example, the "curved membrane" hypothesis of Helmholtz (1869) and the subsequent work of Esser in 1947, were seriously limited. It is difficult to develop a quantitative theory for the eardrum because of the mathematical complexity. In recent years, however, numerical techniques have been used by Funnell (1975) and Funnell and Laszlo (1978) to model the cat eardrum. Through their finite-element modelling they determined that eardrum curvature, conical shape, anisotropy, stiffness and thickness were important model parameters. Funnell (1983) examined the undamped natural frequencies and mode shapes for a cat eardrum, again using the finite-element method. The vibration patterns obtained for the first six natural frequencies are given in Fig. 3.5. The eardrum vibration patterns were found to break up into complex patterns at high frequencies. Results agreed well with Khanna and Tonndorf (1972). Findings suggest that ossicular parameters have little effect on the natural frequencies and mode shapes. Also, the conical shape and possibly the curvature may serve to extend the eardrum frequency range. Funnell, Decraemer, and Khanna (1987) included the effects of damping in the model. Increasing the degree of damping smoothed the frequency response both on the manubrium and on the eardrum away from the manubrium, but the overall level of the displacement amplitude was not significantly decreased. Therefore, it seems that damping results in little loss of the energy being delivered to the middle ear. Instead of using finite-element methods, Rabbitt and Holmes (1986) developed a fibrous dynamic continuum model of the tympanic membrane using asymptotic methods, where the model specifically includes the fibrous ultrastructure of the

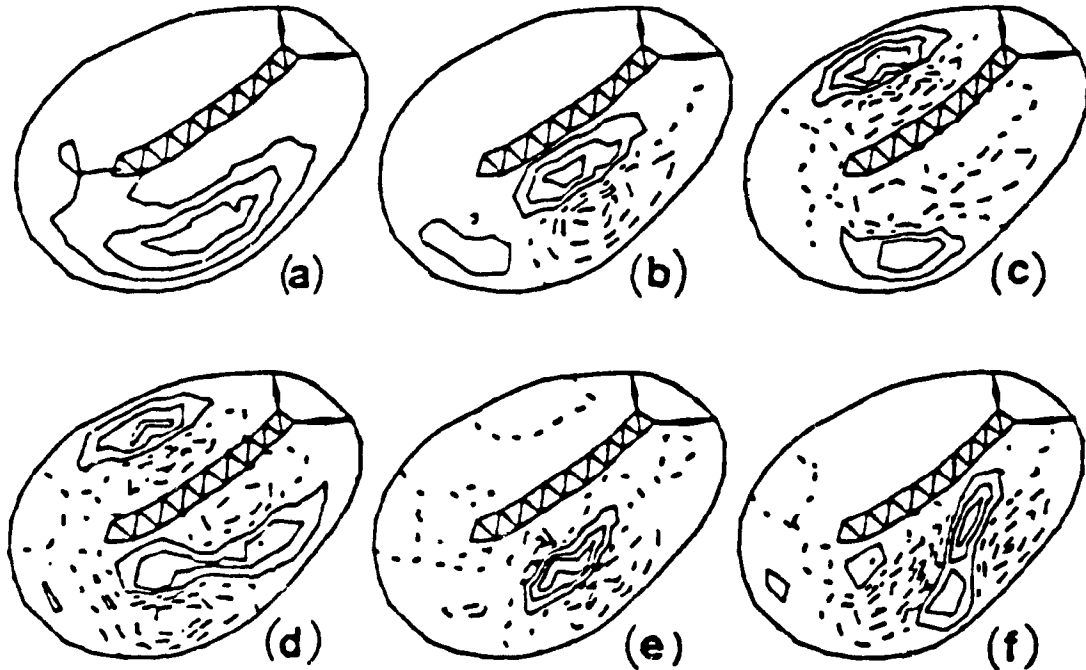


Fig. 3.5

Eardrum vibration patterns determined by the finite-element method for the first six natural frequencies. The contours represent lines of constant vibration amplitude. The solid contours represent positive displacements, the long dashed ones represent negative displacements, and the short dashed lines indicate zero amplitude. (a) 1.761 kHz, (b) 2.312 kHz, (c) 2.590 kHz, (d) 2.622 kHz, (e) 2.926 kHz, (f) 3.194 kHz. From Funnell (1983, p. 1659).

eardrum. The coupling of the ossicular chain and cochlea were included in the model. The asymptotic method involves the development of equations describing the structural damping, transverse inertia and membrane restoring forces which are used in order to incorporate differences in bending, shear, and extensional stiffness across the eardrum. In order to solve the equations, small parameter assumptions must be made. As for any model, accurate geometric and material assumptions are essential for the creation of a successful representation.

3.4 THE MIDDLE EAR

3.4.1 EXPERIMENTS CONCERNING VIBRATION OF THE MIDDLE-EAR OSSICLES

Middle-ear experiments which are of special interest here include those that deal with ossicular vibration. As the manubrium of the malleus is coupled to the eardrum, ossicular loading will also affect the coupled ear canal/eardrum problem. A brief review of some of the more relevant middle-ear experiments follows.

Møller (1963) determined the amplitude and phase angle of the vibrations of the malleus, incus and round window of anaesthetized cats using a capacitive probe. The impedance at the eardrum from 200 to 8000 Hz was also measured. The middle ear was then modelled as a second-order low-pass function, which was valid up to 4 kHz. (It was determined that the eardrum could be modelled as a rigid piston in this region.)

Guinan and Peake (1967) measured ossicular motion of anaesthetized cats using stroboscopic illumination. The stapes was observed to have a linear displacement up to 130 dB SPL. Below 3 kHz, the ossicles moved as one rigid body. At higher frequencies, the stapes and

incus lagged behind the malleus. Guinan and Peake also developed a circuit model to represent the transfer characteristic of the middle ear.

Buunen and Vlaming (1981) measured malleus vibrations in anaesthetized cats using a laser-Doppler velocity meter. Results agreed with those of other studies. Decraemer et al. (1989), who made interferometric measurements of eardrum vibrations in anaesthetized cats, also examined malleus vibrations. It was found that the mode of malleus vibration changed with frequency. Decraemer et al. (1990), using a different interferometric technique, were able to clearly discriminate changes of the malleus vibration response with time.

3.4.2 MIDDLE-EAR MODELS

Lumped-parameter models, which have already been mentioned with respect to the modelling of the ear canal and eardrum, have been frequently applied to the modelling of the middle ear. Onchi (1961), Møller (1961), Zwislocki (1962), and Lynch (1981) among others, have developed circuit models of the middle ear. As an example, the Zwislocki (1962) model will be presented. Zwislocki's analog is based on the functional anatomy of the middle ear. Values of elements were derived from impedance measurements on normal and pathological ears and from anatomical data. The model is valid from 100 Hz to 2 kHz. A schematic block diagram of the middle ear is presented in Fig. 3.6. Block 1 represents the middle-ear cavities. Block 2 simulates the part of the eardrum not coupled to the ossicles. Block 3 represents the coupling between eardrum and ossicles. Block 4 indicates that not all acoustic energy is transmitted across the incudo-stapedial joint. Block 5 introduces the input impedance of the inner ear. The corresponding circuit model is given in Fig. 3.7.

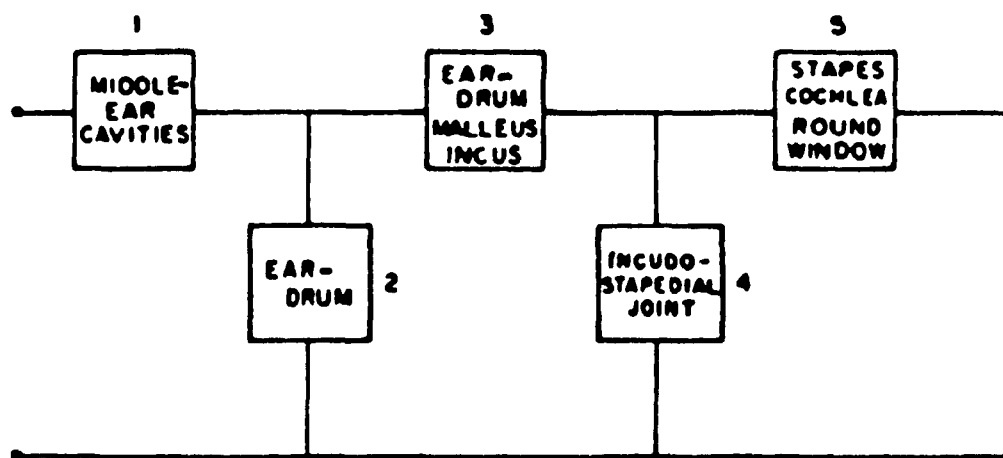


Fig. 3.6

Schematic block diagram of the human middle ear with five functional units.
From Zwislocki (1962, p. 1515).

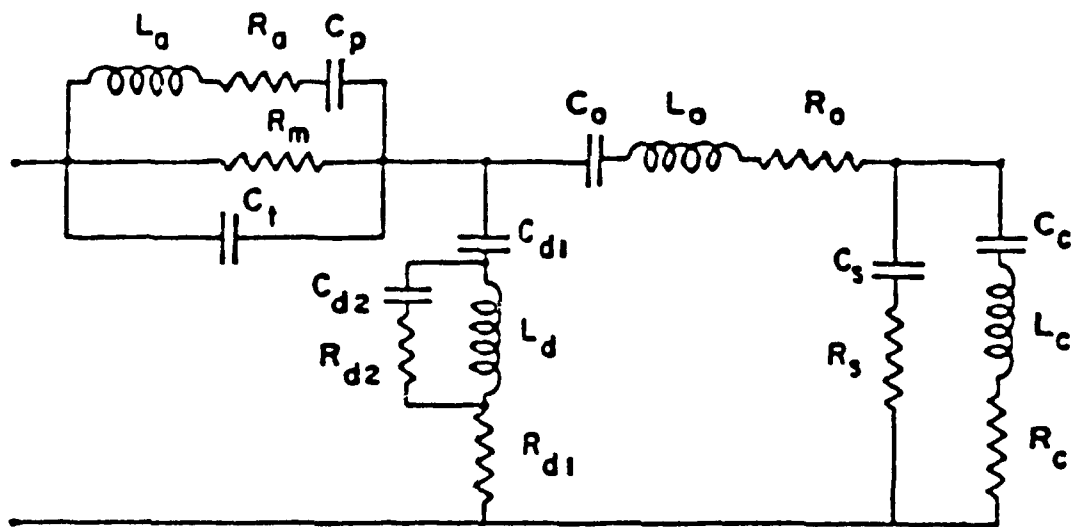


Fig. 3.7

Circuit diagram of the human middle ear. Elements denoted by subscripts a, p, m, and t belong to the middle-ear cavities; those with the subscript d to a portion of the eardrum; those with the subscript o to the malleolar complex; those with the subscript s to the incudo-stapedial joint; and finally those with the subscript c to the cochlear complex. From Zwislocki (1962, p.1520).

3.4 MODELLING THE EAR CANAL/EARDRUM COUPLING

Recent research has considered the importance of coupling between ear canal and eardrum:

Khanna and Stinson (1986) examined energy reflection coefficients in cats. Two cats yielded quite different energy reflection patterns. For one animal, the reflection coefficient rose from 0.22 at 11 kHz to a value of 0.92 at 31 kHz. For the other cat, the reflection coefficient increased to a value of 0.28 at 18.5 kHz and then decreased to a value of 0.05 at 29 kHz. Beyond 30 kHz the reflection coefficient rose steadily to a value of 0.7 at 33 kHz. The fact that in this cat absorption coefficients of 90% were measured at frequencies above 25 kHz emphasizes that the tympanic membrane cannot be treated as rigid. Therefore, in 1989, Stinson and Khanna made further modifications to their theoretical model (modified horn equation including curvature) of 1985. Because of the effects of absorption, the point impedance method of Stinson (1985b) is only useful at frequencies that are not too high. A better representation of the load is necessary to properly predict the sound-pressure distribution in the eardrum vicinity. Stinson and Khanna modified the horn equation by including the motion of the tympanic membrane in the form of a driving term, $F(s)$. The modified horn equation becomes:

$$\frac{d}{ds} \left(A(s) \frac{dp_o(s)}{ds} \right) + k^2 A(s) p_o(s) = F(s) \quad (3.2)$$

The behaviour of the eardrum was simulated using either a mechanically-driven piston or a distributed locally reacting impedance. The theory was tested using model ear canals of uniform cross-section. Thus this testing only took into account the new features of the theory, that is, the

load modelling. Comparison of theory and experimental work indicates that the theory is useful up to 25 kHz in cats and 15 kHz in humans. Sound pressure is assumed to be constant through each cross-section, thus the one-dimensional aspect of the sound field still holds.

Rabbitt and Holmes (1988) studied three-dimensional acoustic waves in the ear canal and their interaction with the tympanic membrane. Although lower acoustic modes travel along the length of the ear canal, higher modes are trapped near the ends of the ear canal, that is, near the concha and near the eardrum. The modes of the pinna result in the complex pressure distribution at the entrance, whereas the complex vibrational shape of the eardrum is responsible for the intricate pressure situation at that end of the canal. Because of the influence of the eardrum, the one-dimensional model of the ear canal is only valid at low frequencies. Thus for validity at high frequencies, a three-dimensional approach is taken. Asymptotic expansions are used to solve the coupled system. The solution is represented by two parts: an outer solution (WKB expansion) valid over most of the length of the canal; and a transition layer, valid near critical resonant cross-sections. As an example, the analysis was applied to a geometry resembling the ear canal and eardrum of a cat. The ear canal, modelled as an axisymmetric tube, was coupled to a flat tympanic membrane, perpendicular to the canal. It was found that at low frequencies, only the plane-wave component mode propagates (refer to Fig. 3.9a). As the WKB expansion is not valid for plane waves at low frequencies, the one-dimensional theory approach was taken to model the (0,0) mode. The new three-dimensional theory introduced rapidly decaying higher modes. However, because of the rapid decay of these modes, the one-dimensional approach remains a reasonable approximation at low frequencies for the given geometry. Also, at 1 kHz, the higher modes only account for a small fraction of the acoustic coupling at the eardrum. This fact is illustrated in Fig. 3.8, where the right-hand axis represents the percent of the total acoustic coupling attributable to the nonplanar modes. The solid curve in the figure, which corresponds

to the model cat eardrum, indicates very little effect at 1 kHz. Nonplanar modes become more important at higher frequencies. For example, at 15 kHz, it can be seen in Fig. 3.9b (comparing to the 1 kHz case in Fig. 3.9a) that trapped modes affect an increasing region of the canal. Higher modes also influence eardrum behaviour. Referring again to Fig. 3.8, the solid curve in the figure indicates that higher modes represent more than 50% of total acoustic coupling above 15 kHz. In summary, multidimensional modes were found to have little effect on the sound pressure in the ear canal for frequencies less than 10 kHz, but were important at higher frequencies. Results indicated that mass loading induced by trapped modes might exceed the magnitude of plane-wave radiation at high frequencies; thus the response of the eardrum may be considerably influenced by nonplanar modes at these frequencies.

Rabbitt (1990) provides a hierarchy of examples illustrating the acoustic coupling of the eardrum. The examples range from a piston coupled to a semi-infinite acoustic duct, to a flexible partition coupled to a semi-infinite variable duct, and to a closed cavity. Results indicate that the acoustics in the ear canal, the eardrum and the secondary middle-ear chambers contribute importantly to the acoustic coupling, limiting passive energy absorption and transmission properties. The work affirms that lumped-parameter models are not suitable at high frequencies.

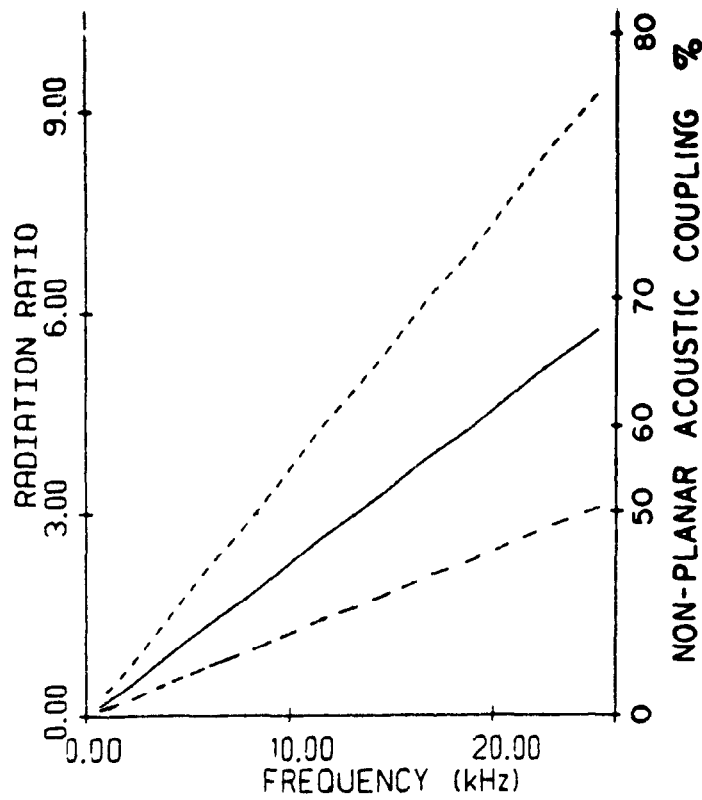


Fig. 3.8

Ratio of plane-wave radiation coefficient to the sum of radiation coefficients for all higher modes (on left vertical axis) and percentage of acoustic coupling of model cat eardrum attributable to nonplanar modes (on right vertical axis). The solid curve corresponds to the model cat eardrum. The top curve corresponds to the same eardrum scaled up to the size of an adult human. The bottom curve corresponds to the eardrum scaled down to that representative of a rabbit. From Rabbitt and Holmes (1988, p. 1072)

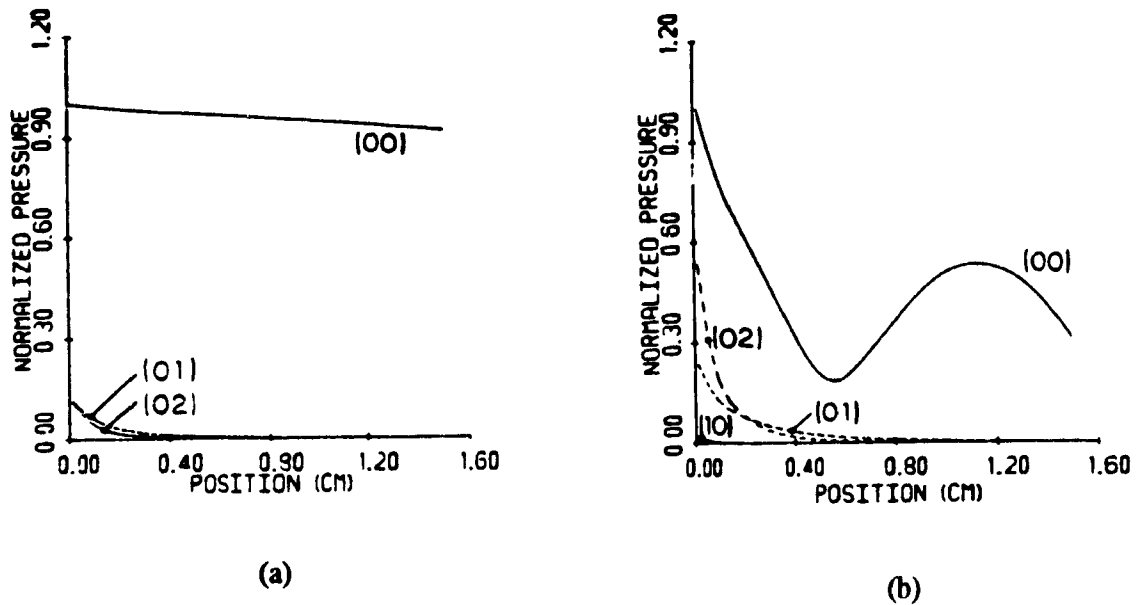


Fig. 3.9

Standing pressure waves in the ear canal. From Rabbitt and Holmes (1988, p. 1075).

(a) Amplitude of modes at 1 kHz.

The plane-wave mode (0,0) is the top curve. Only the plane-wave mode propagates at 1 kHz. The remaining modes are trapped in close vicinity to the eardrum and decay rapidly as the distance from the tympanic membrane is increased. Note that the amplitudes of the nonplanar modes are the WKB solution and the plane-wave result is a numerical solution.

(b) Amplitude of modes at 15 kHz.

The length of the trapped mode zone is extended over about one-third of the length of the ear canal at this frequency. The plane-wave mode is the only propagating wave. All modal amplitudes are the WKB solution.

The WKB solution in (a) and (b) applies to the case of an eardrum coated with a 2 μm thick layer of bronze powder. The coating was found to have little effect at these frequencies.

CHAPTER 4

FINITE-ELEMENT MODELLING

4.1 INTRODUCTION

Problems involving physical systems are often solved by finding a solution that satisfies a differential equation throughout a region. Analytic methods such as separation of variables work well for simple geometries; however, as problems become more complex, different methods must be employed such as the semi-analytic method of conformal mapping or numerical methods. Numerical methods are particularly well-suited to the solution of problems involving more difficult shapes and inhomogeneities. Numerical methods include the finite-difference method, the finite-element method, and the boundary-element method. In the finite-difference method (e.g. Hildebrand, 1968), the derivatives in the partial differential equations are represented by finite-difference approximations. A grid is placed over the structure of interest, and solutions are determined at intersection points. The finite-element method (e.g. Bathe, 1982; Grandin, 1986) involves the division of a region into many simply-shaped subregions so that the solution for each subregion can be represented by a function much simpler than that required for the entire region. The more recently developed boundary-element method (e.g. Brebbia and Dominguez, 1989) involves the discretization of only the surface of the region, whether it is two-dimensional or three-dimensional, as opposed to the finite-element method where in three-dimensional problems the entire volume is discretized.

This chapter is divided into three main sections. The first section presents a basic introduction to the finite-element method, overviewing the mathematical basis and the development of the system matrix equations. The second section explains how standard structural

analysis finite-element code can be altered in order to solve acoustic problems. The third section deals with the concepts involved in fluid-structure interaction, such as the coupled ear canal/eardrum problem, and how the solution is actually implemented using finite-element code, as well as how the output is displayed and, finally, code validation.

4.2 THE FINITE-ELEMENT METHOD

In the finite-element method a system is divided into discrete two- or three-dimensional elements. For example, a plane region may be divided into triangular or quadrilateral elements. A three-dimensional region may be divided into three-dimensional elements such as bricks or tetrahedra. Fig 4.1 illustrates these typical element types. Elements are joined together at points called nodes, and conditions are usually enforced so that each element boundary is compatible with each of its neighbouring elements. The mechanical behaviour of each element is analyzed. This element analysis leads to the formation of a matrix equation relating the behaviour of the element to applied forces. The actual components of each element matrix are dependent upon the shape and material properties of that element. All element equations are then integrated into one complete system matrix equation. The actual nodal responses are determined by solving the system matrix equation using appropriate numerical techniques.

In the following pages, the mathematics which lie behind the above steps are presented, including the determination of the functional, and the subsequent development of the governing finite-element equilibrium equations.

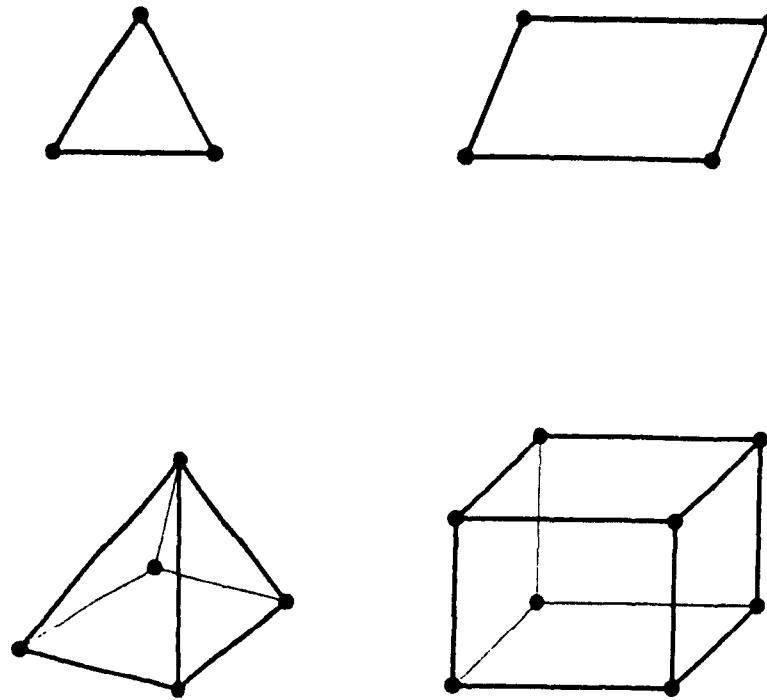


Fig. 4.1

Some typical element types. The triangle and quadrilateral are examples of two-dimensional elements. The tetrahedron and brick are examples of three-dimensional elements.

4.2.1 THE VARIATIONAL FORMULATION AND THE FUNCTIONAL

Finite-element approximations are commonly formulated using the principle of minimum potential energy. The variational principle is expressed as follows: given a functional which represents the potential energy of the system, then the function which minimizes that functional is the solution of the system. For example, the following integral has an integrand involving the variable x , a function $u(x)$ and a derivative of $u(x)$ with respect to x :

$$\Pi = \int_{x_1}^{x_2} f(x, u(x), u'(x)) dx \quad (4.1)$$

The function $u(x)$ (which must satisfy certain boundary conditions) that causes the functional, Π , to be a minimum is the solution.

The variational principle can also be stated as follows: the vanishing of the variation of the functional,

$$\delta\Pi = 0 \quad (4.2)$$

is a necessary condition for the existence of the extreme value of the functional.

A Variational Formulation For Elasticity Problems

Determining functionals can be a very difficult procedure. However, a simple example will be presented here. The principle of virtual work is used as the basis to construct a functional, Π , for equilibrium elasticity problems. Virtual work is defined as work done by a

force undergoing a virtual displacement, which is a variation of the displacement function. The principle states that, for a body in equilibrium, the change in the strain energy resulting from the virtual work of applied loads equals the virtual work:

$$\delta U = \delta W \quad (4.3)$$

If the potential energy (defined as V) of the applied loads is zero at the undeformed condition of the body (i.e. $V_0=0$) then $W = -V$ and equation (4.3) becomes:

$$\delta(U + V) = 0 \quad (4.4)$$

Therefore, comparing equation (4.4) with equation (4.2), it is seen that the functional for the elasticity problem is a sum of the strain energy and the applied load potential energy.

4.2.2 FINITE-ELEMENT EQUILIBRIUM EQUATIONS

Finite-element equilibrium equations are developed using the principle of virtual work described above. The reader is referred to Bathe (1982), p. 120-126, for details regarding the derivation.

Recall from the principle of virtual work that the change in strain energy (the actual stresses, τ , going through the virtual strains, $\bar{\epsilon}$) is equal to the virtual work. Thus:

$$\int_V \bar{\epsilon}^T \tau \, dV = \int_V \bar{U}^T F^B \, dV + \int_S \bar{U}^{s^T} F^S \, dS + \sum_i \bar{U}^{i^T} F^i \quad (4.5)$$

where \bar{U} are the virtual displacements and F^B , F^S and F^i are the external body forces, surface traction forces and concentrated forces, respectively. The superscript S means that surface displacements are considered and the superscript i refers to the displacements at the point where the concentrated forces are applied. For the finite-element method, the above equation is rewritten as a sum of integrals over the volumes and areas of all elements:

$$\begin{aligned} \sum_m \int_{V^{(m)}} \bar{e}^{(m)T} \tau^{(m)} dV^{(m)} = & \sum_m \int_{V^{(m)}} \bar{U}^{(m)T} F^{B(m)} dV^{(m)} \\ & + \sum_m \int_{S^{(m)}} \bar{U}^{S(m)T} F^{S(m)} dS^{(m)} \\ & + \sum_i \bar{U}^i F^i \end{aligned} \quad (4.6)$$

where the superscript m denotes the element m .

At this point a word should be said about the use of two coordinate reference systems in the finite-element method, the global and the local coordinate systems. The global coordinate system is a frame of reference for the entire continuum. The local coordinate system is a system attached to an element. The system is introduced in order to simplify the development of element relationships.

The next step is to define element displacements, strains and stresses in terms of the complete array of finite-element nodal point displacements, that is, in a global sense. Element displacements measured in local coordinates are functions of the global displacements as follows:

$$U^{(m)}(x, y, z) = H^{(m)}(x, y, z) \hat{U} \quad (4.7)$$

where \hat{U} is the vector of global displacements and $H^{(m)}$ is the displacement interpolation matrix. Local element strains, ϵ , are related to global displacements by:

$$\epsilon^{(m)}(x, y, z) = B^{(m)}(x, y, z)\hat{U} \quad (4.8)$$

where $B^{(m)}$ is the strain-displacement transformation matrix. Element stresses are related to strains by:

$$\tau^{(m)} = C^{(m)}\epsilon^{(m)} \quad (4.9)$$

where $C^{(m)}$ is the elasticity matrix, or stress-strain matrix, of the element m . By combining equations (4.7), (4.8), and (4.9) and substituting into equation (4.6), and by imposing unit virtual displacements at all displacement components, one obtains the equilibrium equations for a static analysis. Denoting $\hat{U} = U$ (representing nodal point displacements by U from now on), the equilibrium equation may be written as:

$$KU = F \quad (4.10)$$

where K is the stiffness matrix, U is the vector of nodal point displacements and F is the load vector. The stiffness matrix is found to be:

$$K = \sum_m \int_{V^{(m)}} B^{(m)T} C^{(m)} B^{(m)} dV^{(m)} \quad (4.11)$$

The load vector F includes the effects of the element body forces F_b , element surface forces F_s , element initial stresses F_i , and concentrated loads F_c :

$$\mathbf{F} = \mathbf{F}_B + \mathbf{F}_S - \mathbf{F}_I + \mathbf{F}_C \quad (4.12)$$

and

$$\mathbf{F}_B = \sum_m \int_{V^{(m)}} \mathbf{H}^{(m)T} \mathbf{F}^{B(m)} dV^{(m)} \quad (4.13)$$

$$\mathbf{F}_S = \sum_m \int_{S^{(m)}} \mathbf{H}^{S(m)T} \mathbf{F}^{S(m)} dS^{(m)} \quad (4.14)$$

$$\mathbf{F}_I = \sum_m \int_{V^{(m)}} \mathbf{B}^{(m)T} \boldsymbol{\tau}^{(m)} dV^{(m)} \quad (4.15)$$

where \mathbf{H} is the volume-displacement interpolation matrix, \mathbf{F}^B is a vector of body forces, \mathbf{F}^S is a vector of surface tractions, \mathbf{H}^S is the surface-displacement interpolation matrix, and $\boldsymbol{\tau}$ is the stress vector, and \mathbf{B} is once again the strain-displacement matrix. Note that \mathbf{F}_C is the vector of externally applied forces where the i th component of \mathbf{F}_C is the concentrated force at the i th node.

If one wishes to include the effects of inertia and solve a dynamic problem, element inertia forces are included as part of the body forces \mathbf{F}_B using d'Alembert's principle. The element equilibrium equation becomes:

$$\mathbf{M}\ddot{\mathbf{U}} + \mathbf{K}\mathbf{U} = \mathbf{F} \quad (4.16)$$

where the mass matrix, M , is defined as follows:

$$M = \sum_n \int_{V^{(n)}} \rho^{(n)} H^{(n)T} H^{(n)} dV^{(n)} \quad (4.17)$$

where ρ is the mass density.

Finally, if the effects of damping are to be included, the body forces are again altered and the equilibrium equations become:

$$M\ddot{U} + D\dot{U} + KU = F \quad (4.18)$$

where D is the damping matrix. The damping matrix is usually not assembled from element damping matrices. Rather, the damping matrix is often set equal to some linear combination of the complete system mass and stiffness matrices.

4.2.3 ELEMENT FORMULATIONS

Before discussing the development of different element formulations, it is necessary to introduce a third coordinate system, known as the natural coordinate system. The other two coordinate systems involved in a finite-element analysis are the global and the local coordinate systems as already mentioned. These two systems have the same dimensions. The natural coordinate system on the other hand is dimensionless and identifies positions in an element without regard to element size or shape. As an example, the natural coordinate system for a quadrilateral element is given in Fig. 4.2 below, where the natural axes are defined by r and s .

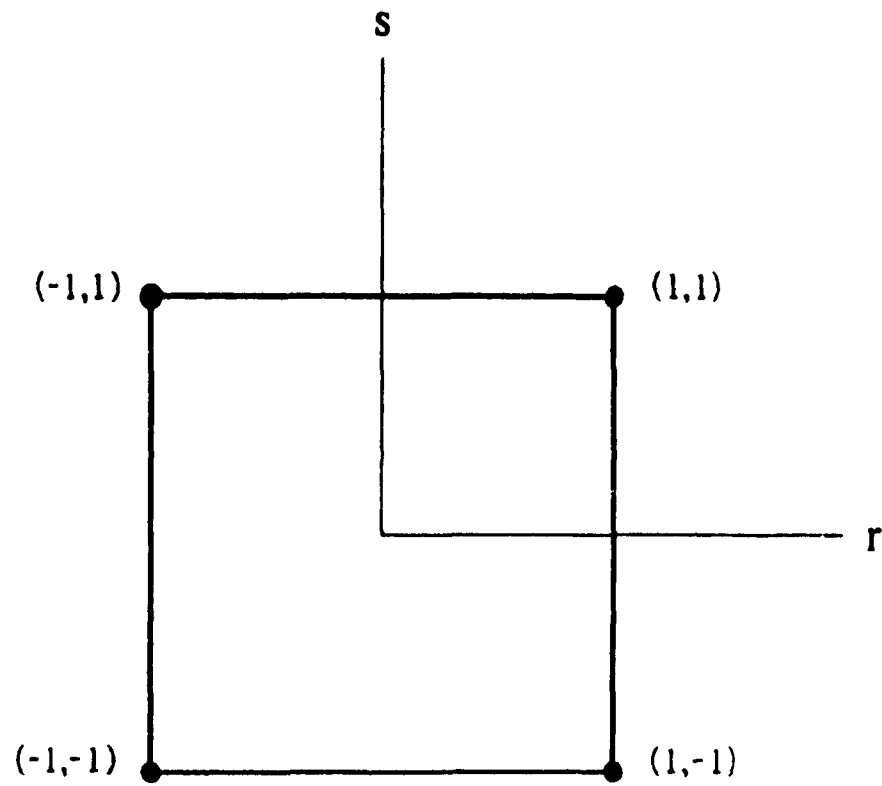


Fig. 4.2

Natural coordinates for the quadrilateral.

There are many different types of elements, both two- and three-dimensional. This chapter describes the formulation of matrices for a general three-dimensional isoparametric element. (Isoparametric elements are elements that use the same basis functions for the spatial coordinate and displacement interpolation formulas.) The problem can easily be reduced to the one-dimensional or two-dimensional case by including only the appropriate coordinate axes. Special mention is made, however, of expressions necessary to implement the quadrilateral element as well as the 8-node brick element — the two element types which are used in this work to model the eardrum and ear canal. Again the reader is referred to Bathe, Chapter 5, for more detailed explanations and derivations.

The first step in developing the element stiffness and mass matrix equations and force vectors is to set coordinate interpolation functions:

$$\begin{aligned} x &= \sum_{i=1}^q h_i x_i \\ y &= \sum_{i=1}^q h_i y_i \\ z &= \sum_{i=1}^q h_i z_i \end{aligned} \quad (4.19)$$

where x , y , and z are coordinates at any point of the element; x_i , y_i , and z_i are coordinates of the q element nodes and the h_i , or shape functions, are defined in the natural coordinate system of the element: for three-dimensional elements the h_i will have variables r , s , and t that vary from -1 to 1; for two-dimensional elements there is no z component, and therefore the natural coordinate system will only include the r and s variables (refer to the quadrilateral element example given in Fig. 4.2). The h_i are unity at node i and zero at all other nodes.

The shape functions for a 2-D quadrilateral element are given by:

$$\begin{aligned}
 h_1 &= \frac{1}{4}(1+r)(1+s) \\
 h_2 &= \frac{1}{4}(1-r)(1+s) \\
 h_3 &= \frac{1}{4}(1-r)(1-s) \\
 h_4 &= \frac{1}{4}(1+r)(1-s)
 \end{aligned}
 \tag{4.20}$$

The shape functions for an 8-node 3-D brick element are given by:

$$\begin{aligned}
 h_1 &= \frac{1}{8}(1-s)(1-t)(1+r) \\
 h_2 &= \frac{1}{8}(1+s)(1-t)(1+r) \\
 h_3 &= \frac{1}{8}(1+s)(1+t)(1+r) \\
 h_4 &= \frac{1}{8}(1-s)(1+t)(1+r) \\
 h_5 &= \frac{1}{8}(1-s)(1-t)(1-r) \\
 h_6 &= \frac{1}{8}(1+s)(1-t)(1-r) \\
 h_7 &= \frac{1}{8}(1+s)(1+t)(1-r) \\
 h_8 &= \frac{1}{8}(1-s)(1+t)(1-r)
 \end{aligned}
 \tag{4.21}$$

As these are isoparametric elements, the same basis functions that were used for the spatial coordinates are also used for the displacement interpolation formulas. The element displacements are then defined as follows:

$$\begin{aligned}
 u &= \sum_{i=1}^q h_i u_i \\
 v &= \sum_{i=1}^q h_i v_i \\
 w &= \sum_{i=1}^q h_i w_i
 \end{aligned}
 \tag{4.22}$$

where u , v , and w are the local element displacements at any point on the element and u_i , v_i , and w_i are the corresponding element displacements at the nodes. Recall that the element stiffness matrix depends on the strain-displacement transformation matrix, B . Strains must be determined in terms of derivatives of nodal displacements with respect to local coordinates. To determine the displacement derivatives, one must evaluate:

$$\begin{Bmatrix} \frac{\partial}{\partial r} \\ \frac{\partial}{\partial s} \\ \frac{\partial}{\partial t} \end{Bmatrix} = \begin{bmatrix} \frac{\partial x}{\partial r} & \frac{\partial y}{\partial r} & \frac{\partial z}{\partial r} \\ \frac{\partial x}{\partial s} & \frac{\partial y}{\partial s} & \frac{\partial z}{\partial s} \\ \frac{\partial x}{\partial t} & \frac{\partial y}{\partial t} & \frac{\partial z}{\partial t} \end{bmatrix} \begin{Bmatrix} \frac{\partial}{\partial x} \\ \frac{\partial}{\partial y} \\ \frac{\partial}{\partial z} \end{Bmatrix}
 \tag{4.23}$$

The above equation can be expressed more concisely as:

$$\frac{\partial}{\partial r} = J \frac{\partial}{\partial x}
 \tag{4.24}$$

where J is the Jacobean operator. Now, solving for spatial derivatives, one obtains:

$$\frac{\partial}{\partial x} = J^{-1} \frac{\partial}{\partial r} \quad (4.25)$$

Using equation (4.22) (the displacement interpolation formulas), and equation (4.25), one evaluates the partial derivatives of u , v , and w with respect to x , y , and z to obtain the strain-displacement transformation matrix, B . Thus we have the elements of the B matrix which are functions of r , s , and t , the natural coordinates. Recall equation (4.6) for the system stiffness matrix. The stiffness matrix for one element is therefore given as:

$$K = \int_V B^T C B dV \quad (4.26)$$

In order to solve for the stiffness matrix as given in equation (4.26), a change of variable must be performed from x , y , z to r , s , t to obtain

$$dV = \det J dr ds dt \quad (4.27)$$

The determination of the stiffness matrix is also dependent upon the constitutive matrix or stress-strain matrix, C . For a plane strain element, such as the quadrilateral element, the stress-strain matrix is defined as follows:

$$C = \frac{E(1-\nu)}{(1+\nu)(1-2\nu)} \begin{bmatrix} 1 & \frac{\nu}{1-\nu} & 0 \\ \frac{\nu}{1-\nu} & 1 & 0 \\ 0 & 0 & \frac{1-2\nu}{2(1-\nu)} \end{bmatrix} \quad (4.28)$$

where ν is Poisson's ratio and E is the modulus of elasticity or Young's modulus.

For a three-dimensional element:

$$C = \frac{E(1-\nu)}{(1+\nu)(1-2\nu)} \begin{bmatrix} 1 & \frac{\nu}{1-\nu} & \frac{\nu}{1-\nu} & 0 & 0 & 0 \\ \frac{\nu}{1-\nu} & 1 & \frac{\nu}{1-\nu} & 0 & 0 & 0 \\ \frac{\nu}{1-\nu} & \frac{\nu}{1-\nu} & 1 & 0 & 0 & 0 \\ 0 & 0 & 0 & \frac{1-2\nu}{2(1-\nu)} & 0 & 0 \\ 0 & 0 & 0 & 0 & \frac{1-2\nu}{2(1-\nu)} & 0 \\ 0 & 0 & 0 & 0 & 0 & \frac{1-2\nu}{2(1-\nu)} \end{bmatrix} \quad (4.29)$$

Finally, numerical integration is used to determine the integral of equation (4.26). For example, using two-point integration for a three-dimensional problem, one obtains:

$$K = \sum_{i,j,k}^2 W_{ijk} F_{ijk} \quad (4.30)$$

where W_{ijk} are the weighting factors, $F = B^T C B \det J$, and F_{ijk} is the matrix F evaluated at points r_i , s_j and t_k .

The element load vectors and mass matrix of equations (4.13), (4.14), (4.15), and (4.17) are easily determined, as the vector of interpolation functions, H , is simply formed of the h_i for the appropriate element type, and other relevant matrices and variables have been determined.

In the final step of the finite-element analysis, element stiffness and mass matrices are inserted into system stiffness and mass matrices, by transferring local element entries to the appropriate global matrix entries.

4.3 AN ACOUSTIC ANALOGY

In order to use existing structural analysis code for an acoustic finite-element analysis, acoustic pressures must be equated in some manner to structural response. The two basic analogies are the displacement-pressure analogy and the stress-pressure analogy as discussed in Lamancusa (1988). For the stress-pressure analogy, the acoustic pressure is equated to the structural stress. The displacement-pressure analogy involves equating the acoustic pressure to the structural displacement. In three dimensions, the stress-pressure formulation results in three degrees of freedom per finite-element mesh point, whereas the displacement-pressure analogy results in one degree of freedom per node. Therefore the displacement approach has the advantage of having fewer unknowns. Also, in the displacement approach, results are directly produced in the form of pressure fields which would be desirable in certain situations. On the other hand, the stress-pressure analogy has the advantage that the predicted structural displacements are equal to the actual acoustical displacements, thus avoiding potential difficulties involved in solving the fluid-structure interaction problem (refer to Section 4.4). However, the stress-pressure analogy suffers from the presence of spurious resonances (Hamdi and Ousset, 1978). These spurious modes can occur with very small frequencies as well as frequencies far from zero, and it is therefore not possible to separate the real modes from the spurious ones. Enforcing irrotationality will cause these unwanted modes to vanish. Hamdi and

Ousset use a penalty method to enforce irrotationality which involves modifying the variational principle for the problem. Lamancusa deals with the spurious mode problem by enforcing irrotational elements. Thus no transverse wave propagation is allowed, and only two-dimensional plane-wave problems can be solved. Considering all of the above factors, it was determined that the displacement-pressure method was the analogy of choice to solve the three-dimensional ear-canal problem. A brief outline of the analogy follows, based on Lamancusa (1988).

The stress-equilibrium equation in one fixed direction (that is x) is described as:

$$\frac{\partial \sigma_x}{\partial x} + \frac{\partial \tau_{xy}}{\partial y} + \frac{\partial \tau_{xz}}{\partial z} = \rho \frac{\partial^2 U_x}{\partial t^2} \quad (4.31)$$

where σ_x is the normal stress component in the x direction, τ_{xy} and τ_{xz} are the shear stress components, ρ is the material mass density, and U_x is the structural displacement in the x direction.

The linearized acoustic wave equation for no losses and no mean flow is:

$$\frac{\partial^2 P}{\partial x^2} + \frac{\partial^2 P}{\partial y^2} + \frac{\partial^2 P}{\partial z^2} = \frac{1}{c^2} \frac{\partial^2 P}{\partial t^2} \quad (4.32)$$

where P is the acoustic pressure and c is the velocity of sound in the fluid.

The essence of the displacement-pressure analogy is to force the structural equation to take on the form of the wave equation. To begin, the displacement in the x direction is set equal to the acoustic pressure, while the displacements in the y and z directions are set to zero:

$$U_x = P \quad (4.33)$$

$$U_y = 0 \quad U_z = 0 \quad (4.34)$$

Now, the three-dimensional isotropic stress-strain relations for a solid are once again considered.

Using Lamancusa's notation, equation (4.9) can be written as:

$$\begin{Bmatrix} \sigma_x \\ \sigma_y \\ \sigma_z \\ \tau_{xy} \\ \tau_{yz} \\ \tau_{zx} \end{Bmatrix} = \begin{bmatrix} \lambda + 2\mu & \lambda & \lambda & 0 & 0 & 0 \\ & \lambda + 2\mu & \lambda & 0 & 0 & 0 \\ & & \lambda + 2\mu & 0 & 0 & 0 \\ & & & G & 0 & 0 \\ & & & & G & 0 \\ & & & & & G \end{bmatrix} \begin{Bmatrix} \epsilon_x \\ \epsilon_y \\ \epsilon_z \\ \gamma_{xy} \\ \gamma_{yz} \\ \gamma_{zx} \end{Bmatrix} \quad (4.35)$$

where $\epsilon_x, \epsilon_y, \epsilon_z$ are the normal strain components, $\gamma_{xy}, \gamma_{yz}, \gamma_{zx}$ are the shear strain components, and G is the modulus of rigidity. The λ and μ are lamé coefficients, defined as follows:

$$\lambda = \frac{\nu E}{(1 + \nu)(1 - 2\nu)} \quad (4.36)$$

$$\mu = \frac{E}{2(1 + \nu)} \quad (4.37)$$

where E is the modulus of elasticity, and ν is Poisson's ratio. The next step involved in the analogy is to set the Poisson's ratio, ν , to zero and to set the modulus of rigidity, G , equal to the

elastic modulus, E . By substituting these values into equation (4.35), and recalling that U_x and U_z have been set to zero, the following equations are obtained:

$$\sigma_x = E e_x = E \frac{\partial U_x}{\partial x} \quad (4.38)$$

$$\tau_{xy} = E \gamma_{xy} = E \frac{\partial U_x}{\partial y} \quad (4.39)$$

$$\tau_{xz} = E \gamma_{xz} = E \frac{\partial U_x}{\partial z} \quad (4.40)$$

Now, using $U_x = P$, and substituting equations (4.38), (4.39), and (4.40) into (4.31):

$$E \frac{\partial^2 P}{\partial x^2} + E \frac{\partial^2 P}{\partial y^2} + E \frac{\partial^2 P}{\partial z^2} = \rho \frac{\partial^2 P}{\partial t^2} \quad (4.41)$$

Finally, equation (4.41) above is identical to equation (4.32) if:

$$c^2 = \frac{E}{\rho} \quad (4.42)$$

In summary then, in order to trick a structural finite-element code to solve an acoustic problem, one must set structural displacements equal to zero in all but one direction, set $\nu = 0$ and $G = E$, and set $E = \rho c^2$ (where ρ will be the desired density of air). Finally, appropriate boundary conditions must be set. On free surfaces, pressure in the selected degree of freedom is set to zero. On rigid walls, no boundary condition is needed. If pressure is known at a certain

node, that node is given a forced displacement equal to the pressure. If the normal component of displacement is known at a certain node, an external force equal to $\rho GAx(t)$ should be applied at this node (where A is the area surrounding the node. Note that this force term is derived and explained in Section 4.4).

4.4 FLUID-STRUCTURE INTERACTION

4.4.1 INTRODUCTION

Most finite-element code available cannot be directly applied to the solution of fluid-structure interaction problems. Some finite-element packages, for example, ANSYS, (Kohnke, 1977), include a fluid element in the possible selection of elements and can handle fluid-solid interaction. However, in most cases, various techniques must be implemented, involving modifications to input data files and alterations to the finite-element code. The development of pre-processing and post-processing programs is also often necessary. Modifications of this kind were necessary for the work undertaken here.

This section introduces the fluid-structure interaction problem. To begin, various methods of dealing with the interaction problem are discussed, followed by the mathematics behind the method chosen, and the actual finite-element implementation. Graphical viewing of the coupled results and code validation are also covered.

4.4.2 APPROACHES TO THE INTERACTION PROBLEM

Fluid-structure interaction problems are typically solved using one of the two approaches mentioned in the previous section (4.3). Either the pressure is used as unknown in the fluid and displacement as unknown in the solid (displacement-pressure analogy), or displacements are used as nodal variables in both the fluid and the structure (stress-pressure analogy). As mentioned in Section 4.3, having displacements as variables in both fluid and structure simplifies the solving of the interaction problem. The other analogy creates difficulties in interaction problems: when the displacement-pressure analogy is employed, special terms must be introduced to couple the pressures of the fluid and the displacement output of the structure. These coupling terms lead to the formation of asymmetric matrices. In the stress-pressure analogy, these terms are not necessary, thus simplifying analysis as well as maintaining matrix symmetry. Papers by Zienkiewicz and Bettess (1978) and Belytschko (1980) review these two methods and their mathematical basis. Olson and Bathe (1985) give a listing of various researchers who have used either one of these approaches. Olson and Bathe themselves presented a formulation for fluid-structure interaction problems based on the fluid velocity potential. Previous work employing a velocity-potential approach had been undertaken by Everstine et al. (1984). In Olson and Bathe's work, velocity potentials are used as nodal variables in the fluid and a hydrostatic pressure variable is introduced and measured at only one node in each fluid region. Displacements are once again the nodal variable in the solid. The resulting matrix equations are banded and symmetric, which makes the velocity-potential approach an interesting alternative to solving the fluid-structure problem, especially for large models.

The displacement-pressure analogy selected in Section 4.3 for the acoustic problem is also a satisfactory approach for the coupled problem, and in comparison with the velocity-

potential approach, has the advantage of being easier to implement with the finite-element code available. The modifications and code development necessary to undertake the interaction problem are now discussed, based on the work of Kalinowski and Nebelung (1982).

4.4.3 SOLUTION OF THE FLUID-STRUCTURE PROBLEM USING EXISTING FINITE-ELEMENT CODE

Kalinowski and Nebelung have developed a method for the solution of fluid-structure interaction problems with the NASTRAN finite-element code. The same approach is, however, applicable to SAP (Bathe, 1974), the structural analysis finite-element package being used in this work. Kalinowski and Nebelung's paper covers the solution of an axisymmetric problem using cylindrical coordinates. Necessary modifications are made in order to solve a general problem in Cartesian coordinates. Initially, finite-element equations are formed for both the acoustic portion and structural portion of the problem:

$$\textit{Fluid Equation: } M^p \ddot{U}^p + D^p \dot{U}^p + K^p U^p = F^p \quad (4.43)$$

(where the superscript p refers to pressure)

$$\textit{Structural Equation: } M\ddot{U} + D\dot{U} + KU = F \quad (4.44)$$

The fluid and structural portions of the problem are merged together to form a complete matrix equation:

$$\begin{bmatrix} M^p & 0 \\ 0 & M \end{bmatrix} \begin{Bmatrix} \dot{U}^p \\ \dot{U} \end{Bmatrix} + \begin{bmatrix} D^p & 0 \\ 0 & D \end{bmatrix} \begin{Bmatrix} \dot{U}^p \\ \dot{U} \end{Bmatrix} + \begin{bmatrix} K^p & 0 \\ 0 & K \end{bmatrix} \begin{Bmatrix} U^p \\ U \end{Bmatrix} = \begin{Bmatrix} F^p \\ F \end{Bmatrix} \quad (4.45)$$

where the upper parts of the matrices correspond to the acoustic part of the problem and the lower parts correspond to the structural part. However, equation (4.45) is not the complete equation for the interaction problem. The essence of fluid-structure interaction is that the pressures on the acoustic side of the problem influence the displacements on the structural side of the problem and vice versa, leading to the development of coupling terms. Solving the coupled problem involves the insertion of special coupling terms into equation (4.45).

To begin, the structural part of the problem is built with elements in the usual finite-element fashion with appropriate material properties and constraints. The acoustic part of the problem is modelled with elements with appropriate material properties and constraints as determined from the acoustic analogy (refer to Section 4.3). A double set of node numbers must be generated at the fluid-structure interface, where nodes on both sides of the interface have the same spatial coordinates. After normal mass, stiffness and damping matrices have been produced, coupling terms are calculated and inserted into the mass and stiffness matrices so that equation (4.45) takes on a new form, where the blocks represent the introduction of the coupling terms:

$$\begin{bmatrix} M^p & \square \\ 0 & M \end{bmatrix} \begin{Bmatrix} \dot{U}^p \\ \dot{U} \end{Bmatrix} + \begin{bmatrix} D^p & 0 \\ 0 & D \end{bmatrix} \begin{Bmatrix} \dot{U}^p \\ \dot{U} \end{Bmatrix} + \begin{bmatrix} K^p & 0 \\ \square & K \end{bmatrix} \begin{Bmatrix} U^p \\ U \end{Bmatrix} = \begin{Bmatrix} F^p \\ F \end{Bmatrix} \quad (4.46)$$

The derivation of these terms and an explicit description of how they are inserted are given below.

Stiffness Matrix Coupling Terms

The stiffness matrix coupling terms have a value of A , representing the surface area surrounding the node. They are due to the pressures at the acoustic interface of the problem acting on the structural interface.

The derivation for the coupling terms for the stiffness matrix is intuitively understood. For the ear canal/eardrum modelling, element surfaces are in the form of four-node quadrilaterals. The pressures exerted by the fluid on the structural part of the problem must be translated to a set of forces normal to the surface:

$$F = pA = \sum \frac{pA_i}{4} \quad (4.47)$$

where F is the force vector applied to a given node, p is the pressure, A_i is the area of the i th element surrounding a given node, and the summation is over all elements attached to that node. The insertion of the coupling terms into the stiffness matrix is effectively equivalent to carrying out equation (4.47).

Stiffness terms are introduced into the stiffness matrix as follows: off-diagonal coupling terms having a value of A , are inserted in the column corresponding to the interface node pressure variable and the row corresponding to the x translational component of the interface structural

node. Similarly, in the column corresponding to the interface node pressure variable and the rows corresponding to the y and z translational components of the interface structural node, coupling terms with the value A_y and A_z are inserted. In the coupling terms, A_x , A_y and A_z are the three components which make up the area vector A , which represents the surface area surrounding the node.

The area surrounding a node is calculated in terms of the areas of all elements surrounding that node. Each surrounding element has a specific area, and a quarter of this area is distributed to each of the four nodes of that element. Therefore, the node in question will receive appropriate area contributions from all elements surrounding it. This procedure is easily implemented in a program by using a DO loop, and by calculating and distributing areas on an element-by-element basis for the entire structure. The area of a quadrilateral element is determined by dividing it into two triangular elements (as in Fig. 4.3) where x_1 , x_2 , x_3 , and x_4 are

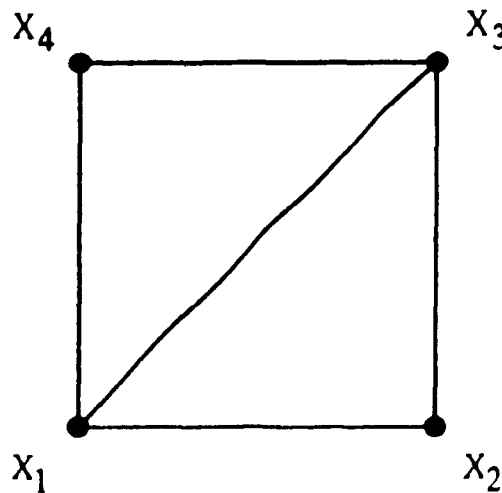


Fig. 4.3

Quadrilateral area determination.

the coordinate vectors of the four nodes of the quadrilateral element and the diagonal arbitrarily runs from x_1 to x_3 . The vector, \mathbf{A} , which is normal to the element with a length that is proportional to the element area, is determined using vector cross products:

$$\begin{aligned} Area_1 &= (x_2 - x_1) \times (x_3 - x_1)/2 \\ Area_2 &= (x_4 - x_3) \times (x_1 - x_3)/2 \\ \mathbf{A} &= Area_1 + Area_2 \end{aligned} \quad (4.48)$$

Mass Matrix Coupling Terms

The mass matrix coupling terms have a value of $-\mathbf{A}\rho G$, where \mathbf{A} represents the surface area surrounding the node, ρ is the fluid density and G is the fluid bulk modulus. The mass matrix coupling terms are due to the mechanical displacements at the structural interface acting on the acoustic interface.

The derivation of the mass matrix coupling terms given below is based on that found in Everstine et al. (1975). To begin, pressure must satisfy the following boundary condition at the fluid-solid interface:

$$\frac{\partial p}{\partial n} = -\rho \ddot{u}_n \quad (4.49)$$

where n is the unit outward normal from the solid at the interface, and ρ is the fluid mass density. Now using the directional derivative of p in the direction of the unit outward normal v from the fluid at a surface point ($v = -n$) and substituting the structural analog u_x for p yields:

$$\frac{\partial u_x}{\partial v} = \nabla u_x \cdot v = \frac{\partial u_x}{\partial x} v_x + \frac{\partial u_x}{\partial y} v_y + \frac{\partial u_x}{\partial z} v_z \quad (4.50)$$

Now, from the acoustic analogy using equations (4.38), (4.39), (4.40), and (4.42), and substituting into equation (4.50):

$$\frac{\partial u_x}{\partial v} = \frac{1}{\rho c^2} (\sigma_{xx} v_x + \tau_{xy} v_y + \tau_{xz} v_z) \quad (4.51)$$

The expression in the parenthesis is equal to the x component of the surface traction vector, T (Cook and Young, 1985). Therefore,

$$\frac{\partial u_x}{\partial v} = \frac{T_x}{\rho c^2} \quad (4.52)$$

If the surface is discretized into a finite number of nodes, the surface traction can be replaced by its lumped equivalent:

$$T_x = \frac{F_x}{A} \quad (4.53)$$

where F_x is the x component of the force applied to a certain node which has an associated area A . Now combining equations (4.52) and (4.53), one obtains:

$$\frac{\partial u_x}{\partial v} = \frac{F_x}{\rho c^2 A} \quad (4.54)$$

Thus, using equation (4.49), and the fact that $n = -v$, the interface condition is obtained:

$$F_x = (\rho c)^2 A \ddot{u}_n \quad (4.55)$$

or, using equation (4.42) and the fact that the modulus of rigidity has been set equal to the elastic modulus in the acoustic analogy, equation (4.55) becomes:

$$F_x = \rho G A \ddot{u}_n \quad (4.56)$$

By inserting the term $-\rho G$ appropriately into the mass matrix, one has effectively accounted for the interface coupling of equation (4.56).

Mass matrix coupling terms are introduced into the mass matrix as follows: off-diagonal coupling terms having a value of $-A_x \rho G$ are inserted in the column corresponding to the x translational component of the interface structural node and the row corresponding to the interface node pressure variable. Similarly, in the columns corresponding to the y and z translational components of the interface structural node and row corresponding to the interface node pressure variable, coupling terms with the value $-A_y \rho G$ and $-A_z \rho G$ are inserted. In the coupling terms, ρ , the fluid density, and G , the fluid bulk modulus, are set as described in the acoustic analogy, and A_x , A_y , and A_z , the three components which make up the area vector A , are identical to those established for the stiffness matrix coupling terms.

Now that the stiffness and mass matrix coupling terms have been determined, the matrix schematic given in equation (4.46) can be completed:

$$\begin{bmatrix} M^p & -A\rho G \\ 0 & M \end{bmatrix} \begin{Bmatrix} \dot{U}^p \\ \dot{U} \end{Bmatrix} + \begin{bmatrix} D^p & 0 \\ 0 & D \end{bmatrix} \begin{Bmatrix} \dot{U}^p \\ \dot{U} \end{Bmatrix} + \begin{bmatrix} K^p & 0 \\ A & K \end{bmatrix} \begin{Bmatrix} U^p \\ U \end{Bmatrix} = \begin{Bmatrix} F^p \\ F \end{Bmatrix} \quad (4.57)$$

4.4.4 IMPLEMENTING THE FLUID-STRUCTURE COUPLING USING SAP

Kalinowski and Nebelung describe how coupling terms can be directly inserted into the mass and stiffness matrices by altering the NASTRAN input file using "DMIG" cards, allowing the coupled problem to be solved entirely within NASTRAN. Unfortunately, this was not possible using SAP, as SAP has nothing similar to NASTRAN's direct matrix insertion capabilities. Therefore, the calculation of the coupling terms, and their insertion into the mass and stiffness matrices, were undertaken in a separate program. First it was necessary to generate mass and stiffness matrices for the uncoupled problem. The ear canal and eardrum parts of the problem were run separately through SAP, thus generating mass and stiffness matrices in the form of equation (4.45). In the specially written code, called LUK, coupling terms are inserted into the matrices. These coupling terms have been calculated by a separate program and output to two files: one for mass coupling terms and one for stiffness coupling terms. The main LUK code asks the user if coupling terms are present. In response to a positive reply, the code reads in the two files which contain coupling terms, as well as equation column and row numbers for each coupled term, and inserts the coupling terms into the matrices appropriately. The user is also questioned as to whether damping should be introduced in the problem. A positive reply

results in the formation of a damping matrix which will have non-zero terms along the diagonal corresponding to nodes for the structural part of the problem. These terms have been calculated by multiplying the mass matrix for the structural part of the problem by some appropriate value. Funnell et al. (1987) have found this mass-proportional damping to produce results most similar to experimentally observed responses. However, stiffness proportional damping or a combination of the two can also be used. For this work, a mass-proportional damping coefficient of 1000 was employed.

At this point, the LUK code has produced mass, stiffness and damping matrices for the coupled problem. The user is then prompted for a frequency at which to perform an analysis. The actual coupled system of equations, as presented in equation (4.57), is then solved. Recall that differentiation of U yields:

$$\begin{aligned}\dot{U} &= j\omega U \\ \ddot{U} &= (j\omega)^2 U = -\omega^2 U\end{aligned}\quad (4.58)$$

Substituting equation (4.58) into (4.57), and assuming that damping is not included in the analysis, it can be seen that the problem will reduce to a system of real linear equations:

$$[K - \omega^2 M]U = F \quad (4.59)$$

On the other hand, if damping is included, a system of complex linear equations is formed:

$$[K - \omega^2 M + D\omega j]U = F \quad (4.60)$$

Therefore, in order to deal with either of these cases, a routine that will solve a system of complex linear equations is employed. A routine from the NAG library (F04ADF) was chosen, which employs the method of Crout factorization to solve the problem (NAG, Mark13, 1988).

4.4.5 VIEWING THE COUPLED RESULTS

An important aspect of finite-element analysis is the post-processing necessary to view results, involving some sort of graphics program. In our laboratory, a graphics program known as CON has been developed by Funnell to view results from a SAP analysis. This program reads in necessary data from the SAP results file to produce contour plots for acoustical or mechanical problems. Obviously the output produced by NAG within the LUK code will not be in a format immediately ready for graphics viewing. For example, coupled output is in the form of real and imaginary parts and different element types are involved. The modifications necessary in order to view this output by CON are explained here. Similar sorts of manual manipulations would be necessary for any graphics package which uses SAP output files to view results.

As stated, the output produced by NAG consists of real and imaginary nodal output for the entire problem (note that it is also possible, by slightly altering code, to output phase and amplitude components instead). To begin, in the main LUK code, the acoustic nodal output is separated from the structural nodal output. The real and imaginary components for both parts of the problem are then output separately to two files, producing four files in all. In order to view these four files, they have to be in proper file format to be read by the graphics program. For example, in order to view the real part of the acoustics output, it is necessary to insert the real acoustic nodal output file into the displacement section of a normally structured SAP output file, which has been produced by running only the acoustic part of the problem through SAP.

Similarly, to view either the real or imaginary structural output, the appropriate file is inserted into normally structured SAP output files obtained by running only the structural problem through SAP. These new files then contain all important nodal and element definitions necessary for the plotting of structures as well as correct output obtained from running the coupled problem. Most importantly, these files are structured in a way that the graphics program CON will accept them.

4.4.6 CODE VALIDATION

Unfortunately, we have not found an appropriate three-dimensional coupled problem with an analytical solution in order to check fully the validity of the coupling concepts as presented in the theory section and the finite-element implementation. Nevertheless, various checks were performed on the code to ensure its correctness. Preliminary checking of the coupled program code, LUK, included running the example presented in the Kalinowski paper. Results obtained were in good agreement with those of the paper. Following this, various internal checks were performed on the code using the ear canal/eardrum problem. To begin, NAG output was compared with SAP output for the static case. The acoustic pressure output at the ear canal/eardrum interface determined by running the coupled problem through LUK was used as force input to the eardrum problem alone — which was then run through SAP. Displacements obtained on the eardrum were the same as those obtained by NAG for the coupled problem. Similarly, the displacement data from the eardrum part of the coupled output were converted to force input for the end of the ear canal, and the ear canal problem was run separately through SAP. Output ear canal pressures were the same as those obtained by NAG for the coupled problem. Similar internal checking was successfully performed when inertial and damping effects were included.

CHAPTER 5

FINITE-ELEMENT MODEL TESTS AND RESULTS

5.1 INTRODUCTION

This chapter presents the results of the initial attempts made at modelling the coupled ear canal/eardrum problem using the finite-element method. To begin, geometric simplifications which were employed to model both eardrum and ear canal are presented, as well as mesh size and associated material properties. The preliminary model does not represent the exact geometric characteristics of the coupled system. Its purpose is to test the implementation of the fluid-structure theory, using a system which resembles that of the coupled eardrum/ear canal, but that does not require the more complicated computerized three-dimensional reconstruction and meshing techniques that would be necessary in the ideal modelling case. To begin analysis, the eardrum/ear canal system is uncoupled. An eigenvalue analysis is performed on both the ear canal and eardrum, treating them as separate problems. Results for these analyses are presented, and as there are theoretical solutions for the individual models due to their regular geometric shape, results are compared to theory. The coupled problem is then dealt with. Output obtained for a forced response analysis performed at several frequencies is presented, followed by a discussion of these results.

5.2 THE FINITE-ELEMENT MODEL OF THE EAR CANAL AND EARDRUM

5.2.1 EARDRUM SHAPE AND PROPERTIES

In order to simplify the geometry of the coupled problem, the eardrum is modelled as a flat circular plate of radius 3.5 mm, lying in the y-z plane. Thus the model does not include eardrum curvature, which is an essential feature in proper eardrum modelling. The eardrum model has a thickness of 40 μm , an elastic modulus of $4 \times 10^8 \text{ N/m}^2$, a Poisson's ratio of 0.3 and a density of 1000 kg/m^3 . Values for Poisson's ratio, density and thickness are the same as those used in Funnell's 1983 eigenvalue eardrum analysis. In order to obtain reasonable displacements when the eardrum is modelled as a flat or a shallow cone, a greater stiffness is required. To account for the lack of curvature in this model, the elastic modulus value is about 20 times the value used by Funnell ($2 \times 10^7 \text{ N/m}^2$). [Note that in Funnell (1983) and Funnell et al (1987) the elastic modulus is incorrectly given as $2 \times 10^9 \text{ N/m}^2$. In both cases, the value actually used was $2 \times 10^7 \text{ N/m}^2$.] Nodes along the circumference of the eardrum model are completely constrained. All other nodes have five degrees of freedom, including x, y, and z translation and y and z rotation.

5.2.2 EAR CANAL SHAPE AND PROPERTIES

To simplify the geometrical shape of the ear canal, it is modelled as a cylindrical tube, with a length of 26 mm and a radius of 3.5 mm. The density is set at 1.21 kg/m^3 and the elastic modulus is set to $1.42 \times 10^5 \text{ N/m}^2$ (air at 20°C). As mentioned in Section 4.2, certain material

properties in the finite-element file must be set appropriately to apply the acoustic analogy. Therefore, Poisson's ratio is set to 0.0 and the bulk modulus is set equal to the elastic modulus at $1.42 \times 10^9 \text{ N/m}^2$. Nodes on the surface at the open end of the canal are completely constrained. All other nodes have one degree of freedom corresponding to x translation.

5.2.3 FINITE-ELEMENT MESHES FOR THE EARDRUM AND EAR CANAL

The finite-element mesh for the flat circular eardrum consists of 49 quadrilateral elements. The mesh for the eardrum is formed by mapping a uniform 7-element by 7-element square onto a circle. The mesh for the cylindrical ear canal consists of 343 8-node brick elements. The cross-section of this mesh is identical to that of the eardrum, and the mesh has a longitudinal depth of seven elements.

Fig. 5.1 presents the finite-element meshes for the initial models of eardrum and ear canal. Obviously the mesh of the end face of the ear canal is identical to the eardrum mesh. The nodes on the two surfaces share the same coordinates in space, thus establishing the double-node interface which is necessary in order to solve the coupled problem as described in Chapter Four.

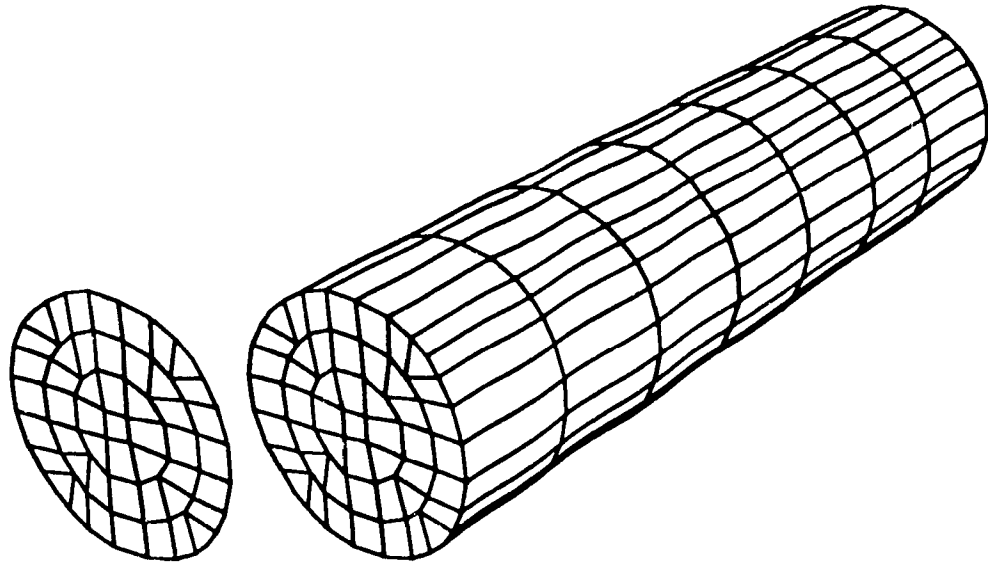


Fig. 5.1

Finite-element meshes for the eardrum (represented by a flat plate) and the ear canal (represented by a cylindrical tube).

5.3 EIGENVALUE ANALYSIS OF THE UNCOUPLED PROBLEM

An eigenvalue analysis was performed on each part of the uncoupled system in order to determine undamped natural frequencies and mode shapes. This involves the solution of the following equation:

$$KU - \omega^2 MU = 0 \quad (5.1)$$

where ω is the frequency.

5.3.1 THE EARDRUM

The first six modes of vibration obtained for the finite-element analysis of the eardrum (circular plate) are shown in Fig. 5.2. This figure and all subsequent figures in this chapter were generated using CON. For the eardrum problem, CON produces contour lines of equal displacement amplitude by linearly interpolating between calculated nodal displacements. The thin black lines correspond to positive displacement contours; the thin grey lines correspond to negative displacement contours; and the thick black lines to zero displacement.

In Fig. 5.2, the first mode occurs at around 1 kHz, which is similar to that determined by Funnell (1983) for his eardrum model. (As stated previously, this was accomplished by adjusting the elastic modulus, E .)

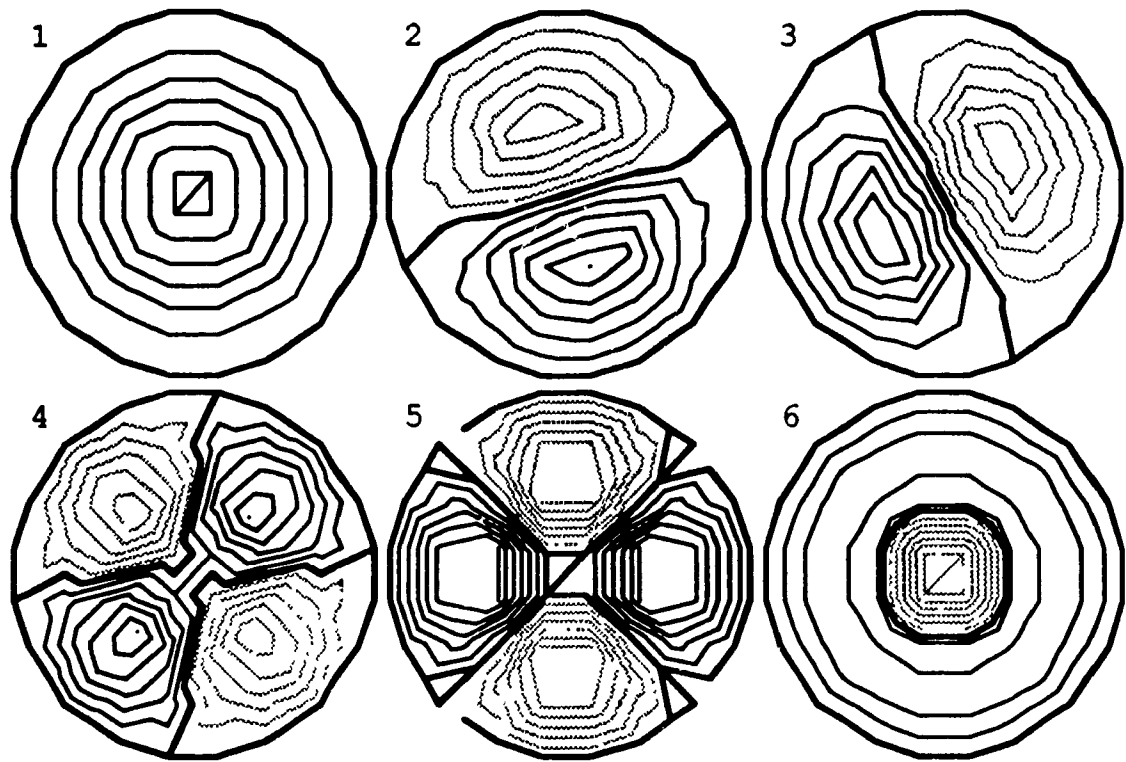


Fig. 5.2

Eigenvalue analysis of the eardrum (circular plate). The first six modes have the following frequencies: 1) 1.02 kHz, 2) 2.197 kHz, 3) 2.197 kHz, 4) 3.527 kHz, 5) 3.833 kHz, and 6) 4.017 kHz.

The formula to determine the theoretical eigenvalues of a uniform circular plate is given by:

$$f_{mn} = \frac{\pi h}{2a^2} \sqrt{\frac{E}{3\rho(1-\nu^2)}} (\beta_{mn})^2 \quad (5.2)$$

where the subscript mn refers to the (m,n) th mode and the β_{mn} are:

$$\begin{aligned} \beta_{01} &= 1.015, & \beta_{02} &= 2.007, & \beta_{03} &= 3.000 \\ \beta_{11} &= 1.468, & \beta_{12} &= 2.483, & \beta_{13} &= 3.490 \\ \beta_{21} &= 1.879, & \beta_{22} &= 2.992, & \beta_{23} &= 4.000 \\ & & & & & \text{etc.} \end{aligned} \quad (5.3)$$

and E is the modulus of elasticity, ν is the Poisson's ratio, ρ is the density, h is the half-thickness of the plate, and a is radius of the plate (Morse and Ingard, 1968, p.215-216). The finite-element output values can be compared with theoretical values in the table below.

m,n	Finite-element frequency (kHz)	Theoretical frequency (kHz)	% Error
0,1	1.02	1.016	0.39
1,1	2.197	2.114	3.93
1,1	2.197	2.114	3.93
2,1	3.527	3.469	1.67
2,1	3.833	3.469	10.49
0,2	4.017	3.955	1.57

Table 5.1 Finite-element and theoretical frequencies for the first six modes of the eardrum.

Note the presence of degenerate modes in Table 5.1. As degenerate modes, modes (1,1) and (2,1) have two eigenvectors for each frequency. In Fig. 5.2, the finite-element method result for mode (1,1) is presented in Case 2 and Case 3. Case 2 and Case 3 have the same frequency, that is, 2.197 kHz. Note that there is a rotation of 90° between the two patterns. They are the same because the finite-element mesh used to model the circular eardrum exhibits 90° symmetry. On the other hand, Case 4 and Case 5 which correspond to mode (2,1) do not have identical frequencies (Case 4: 3.527 kHz, Case 5: 3.833 kHz). Note that there is a rotation of 45° between the two patterns. As the finite-element mesh does not exhibit 45° symmetry, it splits this mode.

By examining Table 5.1, it can be seen that the percentage error between finite-element and theoretical frequency differs for different modes. This is because the mesh has greater difficulty in accurately determining the modes which are more complex. An important factor that must be considered in finite-element modelling is the resolution or fineness of the mesh. A finer mesh generally produces more accurate results than a coarse one, but there are other considerations as well. For example, a mesh of a given resolution may only allow a certain number of modes to be resolved in an eigenvalue analysis. In fact, using the 49-element mesh developed here, it was only possible to resolve the first six modes as presented in Table 5.1 and Fig. 5.2. To experiment, a finer mesh of the eardrum was generated (using a 9-element diameter). With this mesh it was possible to resolve many higher modes, as well as increase accuracy. However, one must also consider the fact that computer storage requirements and run time increase with increasing mesh resolution. In this work, the 49-element mesh produced results of sufficient accuracy for our purposes, and was therefore employed.

5.3.2 THE EAR CANAL

The first six modes obtained for an eigenvalue analysis of the ear canal (cylindrical tube) are shown in Fig. 5.3. Here the thin black lines correspond to positive pressure contours; the thin grey lines correspond to negative pressure contours; and the thick black lines correspond to zero pressure contours. The first five modes are longitudinal modes, that is, pressure variations exist only along the longitudinal axis. The sixth mode, which occurs at about 27 kHz, is the first transverse mode, that is, where variations occur in the plane perpendicular to the longitudinal axis.

The theoretical natural frequencies for the longitudinal modes of a cylindrical tube closed at one end are given by:

$$f_n = \frac{2n-1}{4} \frac{c}{L} \quad n = 1, 2, 3, \dots \quad (5.4)$$

where c is the speed of sound, and L is the length of the tube (Morse and Ingard, 1968, p. 474).

The longitudinal mode results determined from the finite-element acoustic analogy are compared to theoretical values in the table below:

n	Finite-Element Frequency (kHz)	Theoretical Frequency (kHz)	% Error
1	3.287	3.298	0.33
2	9.696	9.894	2.00
3	15.62	16.49	5.28
4	20.76	23.09	10.09
5	24.86	29.68	16.24

Table 5.2 Finite-element and theoretical frequencies for the first five longitudinal modes of the ear canal.

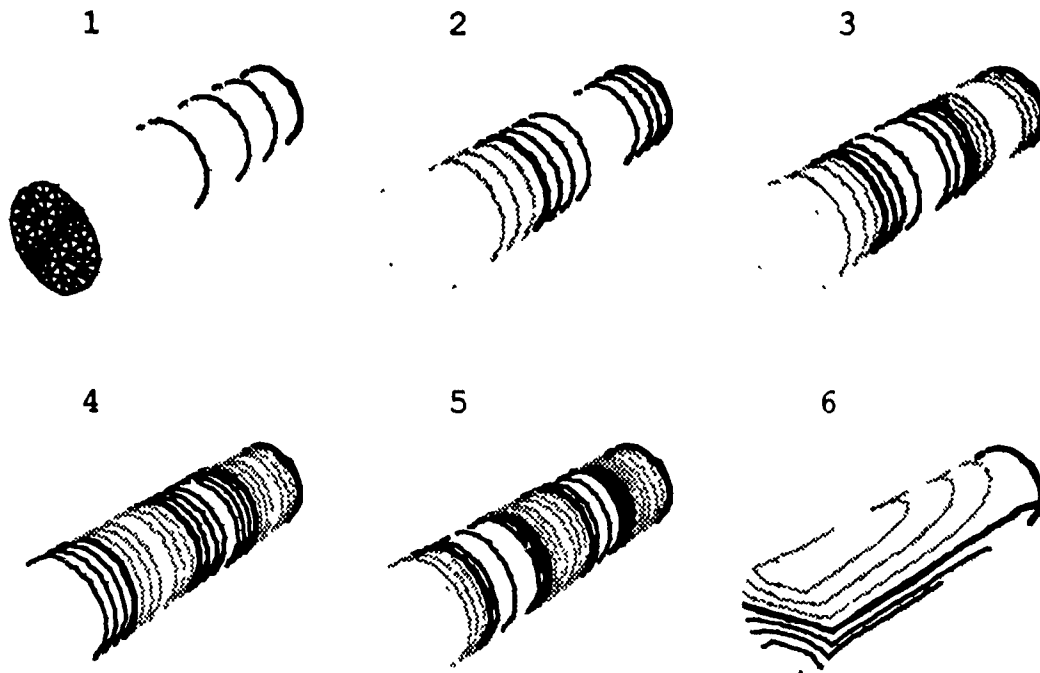


Fig. 5.3

Eigenvalue analysis of the ear canal (cylindrical tube). The first six modes have the following frequencies: 1) 3.287 kHz, 2) 9.696 kHz, 3) 15.62 kHz, 4) 20.76 kHz, 5) 24.86 kHz, and 6) 28.53 kHz. Note that in Case 1, because the distribution is uniform across the ear canal, all the surface nodes on the near end are joined together by the contour line.

The theoretical natural frequencies for the transverse modes of a circularly cylindrical tube are given by:

$$f_{mn} = \frac{\alpha_{mn}c}{2b} \quad (5.5)$$

where $\alpha_{m,n}$ for the (m,n) th mode are:

$$\begin{aligned} \alpha_{10} &= 0.5861, & \alpha_{20} &= 0.9722 \\ \alpha_{01} &= 1.2197, & \alpha_{11} &= 1.6970 \\ & & & \text{etc.} \end{aligned} \quad (5.6)$$

and b is the radius of the circular tube (Morse and Ingard, 1968, p.511).

The first transverse mode result determined from the finite-element acoustic analogy compares well to the theoretical value:

m,n	Finite-Element Frequency (kHz)	Theoretical Frequency (kHz)	% Error
1,0	28.53	28.72	0.66

Table 5.3 Finite-element and theoretical frequency for the first transverse mode of the ear canal.

Note the increasing percentage error with increasing frequency in the longitudinal modes. However, the result for the first transverse mode, which occurs at about 28 kHz, is very accurate. Although the frequency is quite high, the first transverse mode is not complex, and the 49-element mesh is sufficiently fine to resolve it.

5.4 RESULTS FOR THE COUPLED PROBLEM

5.4.1 INTRODUCTION

In this section results obtained for the coupled eardrum/ear canal problem are presented. Using SAP in conjunction with the special code developed as described in Chapter Four, harmonic forced response analyses were performed at several frequencies. Note that running the coupled problem (on a VAXstation 3520) at a single frequency and displaying results took from 30 to 45 minutes.

Due to the form of the output, which is four plots per run (real and imaginary parts for both plate and tube sections), it is not feasible to give a complete description of the coupled problem behaviour over the entire frequency range of interest. The problem was solved for approximately twenty different frequencies, with a constant pressure field of 2.828 N/m^2 acting over the surface nodes at the entrance to the canal. (This is the zero-to-peak pressure variation equivalent to 100 dB SPL.) The results for three frequencies will be presented in this section: 100 Hz, 3.5 kHz, and 7.1 kHz. These frequencies were chosen with the aim of presenting some interesting aspects of the coupled problem by comparing coupled output with eigenvalue output obtained from the uncoupled problem.

5.4.2 RESULTS AT INDIVIDUAL FREQUENCIES

A. 100 Hz

Coupled results for 100 Hz are presented in Fig. 5.4. At very low frequencies a simple low-order vibration pattern appears on the eardrum. This is to be expected considering the

uncoupled results for both the ear canal and eardrum. The first uncoupled eardrum mode does not appear until approximately 1 kHz, and the first mode of the ear canal appears at about 3 kHz. Note the very small size of the imaginary component relative to the real component for the ear canal and eardrum. The imaginary component of the eardrum displacement is smaller than the real component by a factor of more than 10^3 (Fig. 5.4b and a). These small imaginary components are expected at such a low frequency where damping will have little effect on the problem. In the ear canal as the pressure travels down the tube, the real component is effectively constant, increasing from 2.828 to 2.843 N/m² (Fig. 5.4c).

B. 3.5 kHz

Results obtained for the coupled problem at 3.5 kHz are presented in Fig. 5.5. This more complex, circular mode appears at about 4 kHz in the uncoupled drum problem. In examining the real and imaginary parts of the eardrum in Fig. 5.5a and b, one notices the increasing effects of damping: for the point of maximum positive displacement, the imaginary component is now approximately 47% of the real component. Damping effects are also present in the ear canal: at the eardrum end, the imaginary ear-canal pressure component has become quite large, reaching about 55% of the real ear-canal pressure component (Fig. 5.5d and c). In Fig. 5.5c, the real pressure changes from 2.828 at the ear-canal end to -24.83 N/m² at the eardrum end, where the zero pressure contour is just inside the opening. This is similar to the first longitudinal mode for the uncoupled tube which contains a quarter wavelength. Note that the negative real components of the eardrum displacements and of the ear-canal sound pressures reflect increasing inertial effects.

C. 7.1 kHz

An interesting higher-order mode appears for the coupled problem at 7.1 kHz (refer to Fig. 5.6). As mentioned previously, it was not possible to resolve any more than the first six modes for the uncoupled drum problem with the mesh resolution being used. However, this mode appears to be a combination of theoretically predicted modes (4,1) and (4,2). Using Equation 5.2, mode (4,1) would in theory have a frequency of about 6.9 kHz. Note that for the uncoupled canal problem, the first transverse mode does not appear until about 27 kHz. The real pressure component of the tube contains a half wavelength from 2.828 to -2.827 N/m². This is similar to the half-wavelength mode for an uncoupled tube closed at both ends, which would occur at about 6 kHz (half-way between the 3 and 9 kHz of the first two modes of the uncoupled tube open at one end). Once again the imaginary component in plate and tube (Fig. 5.6b and d) reflects the influence of damping. The imaginary part of the tube output which ranges from -0.0294 to 0.0259 N/m² (see Fig. 5.6d) is very interesting. The higher-order mode is seen to be trapped at the end. Therefore, Fig. 5.6d provides an example of a non-propagating higher order mode as discussed in Rabbitt and Holmes (1988).

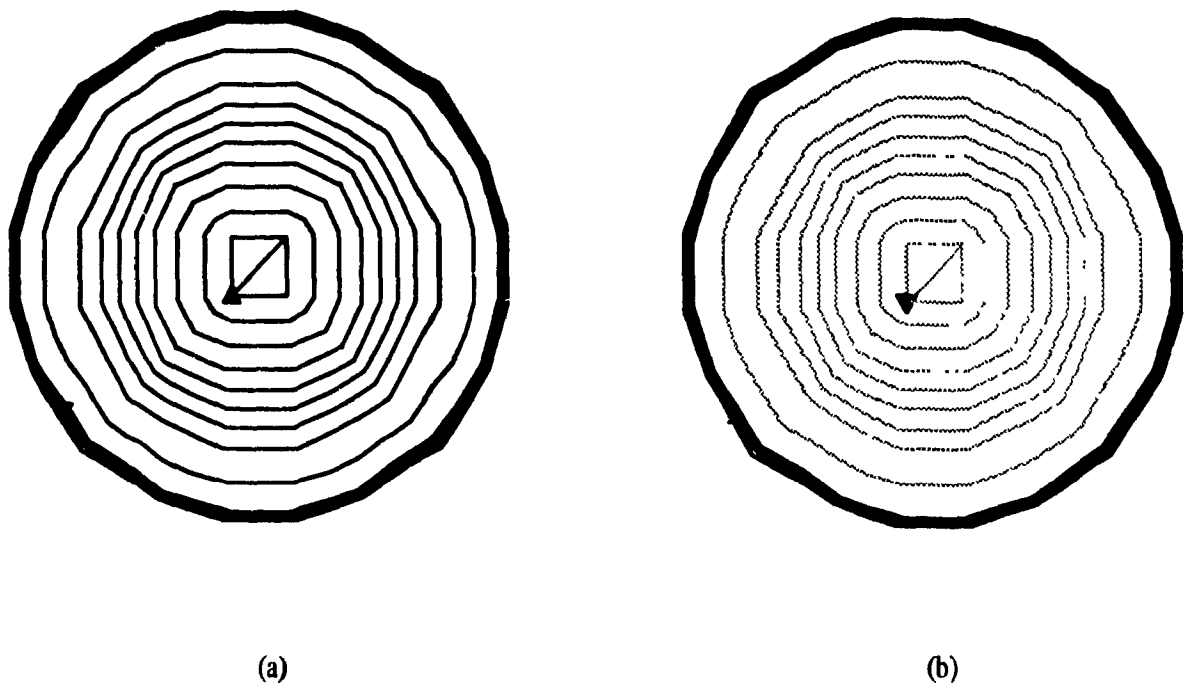


Fig. 5.4

Results for the coupled problem at 100 Hz.

(a) Eardrum: real component. Range: 0.0 m to 2.702 μm .
Contour lines are spaced at intervals of 0.300 μm .

(b) Imaginary component for the eardrum. Range: -43.33 nm to 0.0 m.
Contour lines are spaced at intervals of 4.814 nm.

Note that in these and the following eardrum figures, the black upward pointing triangle corresponds to the contour of most positive displacement, and the downward pointing triangle corresponds to the contour of most negative displacement.

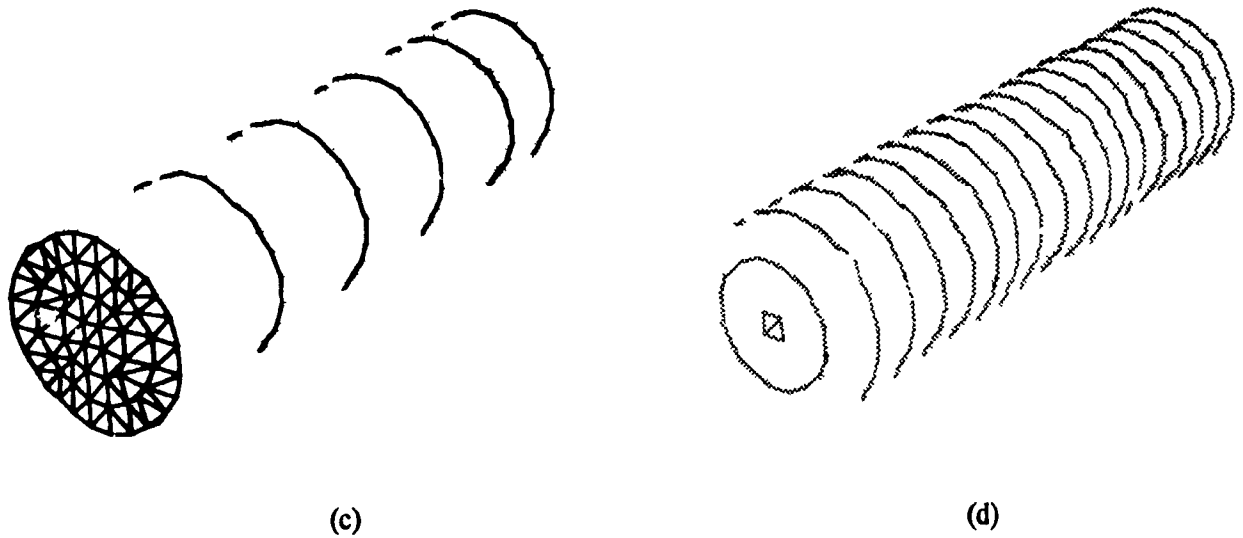


Fig. 5.4 (Continued)

Results for the coupled problem at 100 Hz.

(c) Ear canal: real component. Range: 2.828 N/m^2 to 2.843 N/m^2 .
Contour lines are spaced at intervals of $2.843 \times 10^{-3} \text{ N/m}^2$.

(d) Ear canal: imaginary component. Range: $-186.6 \times 10^{-6} \text{ N/m}^2$ to $-9.728 \times 10^{-12} \text{ N/m}^2$.
Contour lines are spaced at intervals of $9.821 \times 10^{-6} \text{ N/m}^2$.

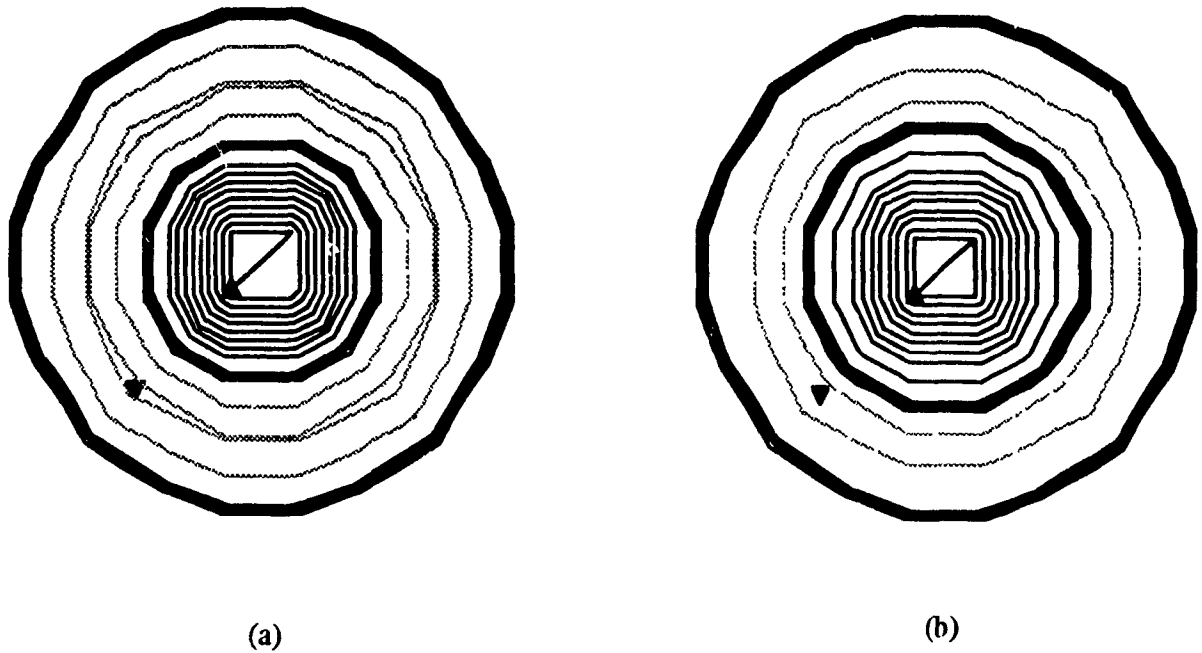


Fig. 5.5

Results for the coupled problem at 3.5 kHz.

(a) Eardrum: real component. Range: $-1.554 \mu\text{m}$ to $6.226 \mu\text{m}$.
Contour lines are spaced at intervals of $0.692 \mu\text{m}$.

(b) Eardrum: imaginary component. Range: -496.5 nm to $2.91 \mu\text{m}$.
Contour lines are spaced at intervals of $0.323 \mu\text{m}$.

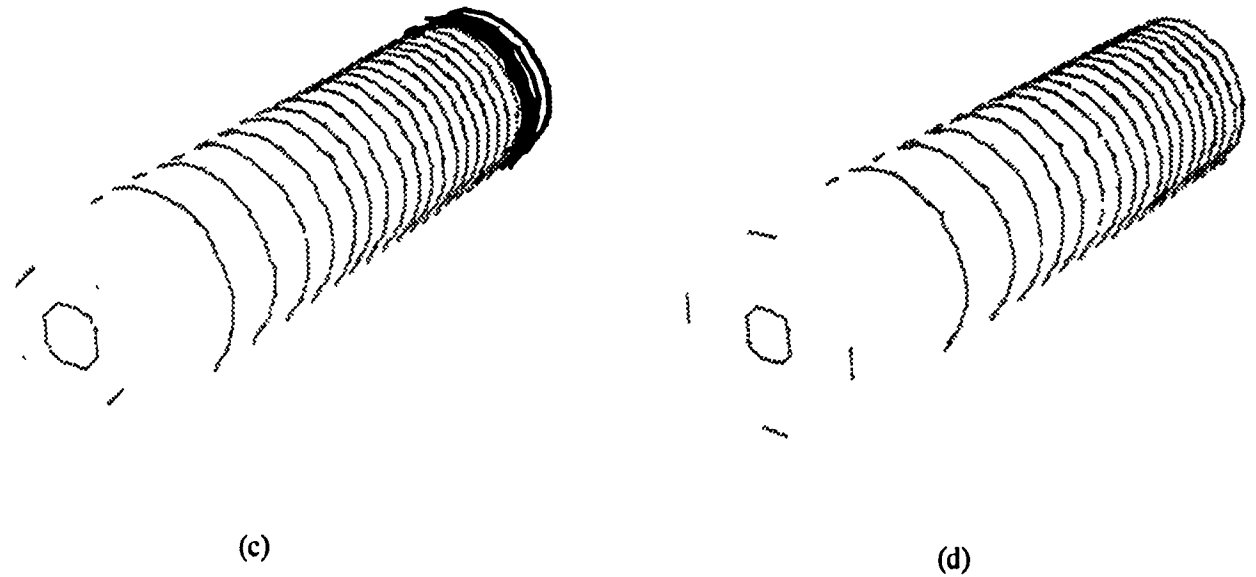


Fig. 5.5 (Continued)

Results for the coupled problem at 3.5 kHz.

(c) Ear canal: real component. Range: -24.83 N/m^2 to 2.828 N/m^2 .
Contour lines are spaced at intervals of 1.307 N/m^2 .

(d) Ear canal: imaginary component. Range: -14.01 N/m^2 to $-1.259 \times 10^9 \text{ N/m}^2$.
Contour lines are spaced at intervals of 0.737 N/m^2 .

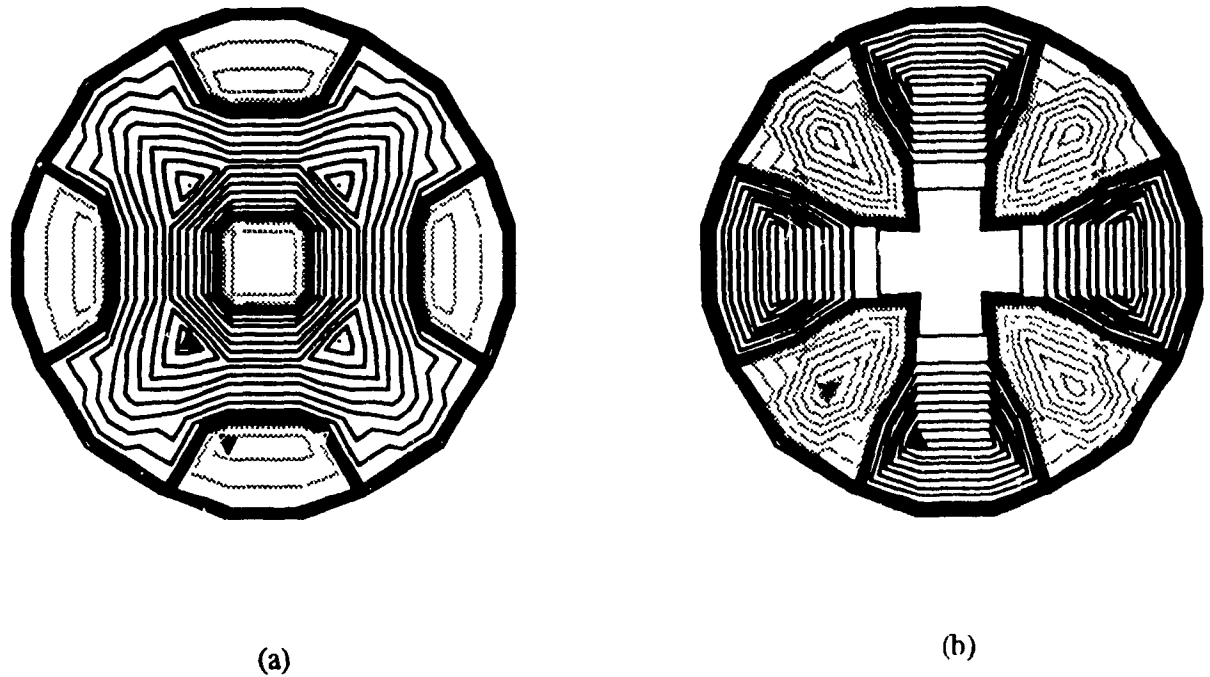


Fig. 5.6

Results for the coupled problem at 7.1 kHz.

(a) Eardrum: real component. Range: -29.87 nm to 102.3 nm.
Contour lines are spaced at intervals of 11.367 nm.

(b) Eardrum: imaginary component. Range: -22.09 nm to 25.23 nm.
Contour lines are spaced at intervals of 2.803 nm.

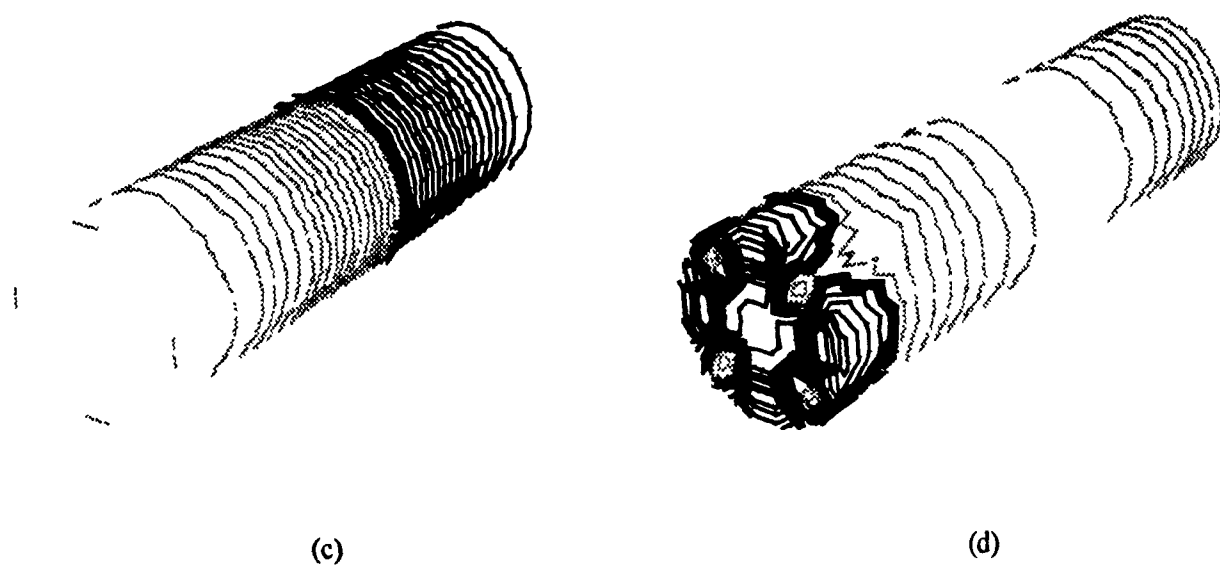


Fig. 5.6 (Continued)

Results for the coupled problem at 7.1 kHz.

(c) Ear canal: real component. Range: -2.87 N/m^2 to 2.828 N/m^2 .
Contour lines are spaced at intervals of 0.151 N/m^2 .

(d) Ear canal: imaginary component. Range: $-29.44 \times 10^3 \text{ N/m}^2$ to $25.87 \times 10^3 \text{ N/m}^2$.
Contour lines are spaced at intervals of $3.271 \times 10^3 \text{ N/m}^2$.

CHAPTER 6

CONCLUSIONS

6.1 SUMMARY OF CONTRIBUTIONS

A method has been presented to deal with the problems involved in coupling the acoustical behaviour of the ear canal with the mechanical behaviour of the eardrum. The method involves the use of the SAP finite-element package, the use of an acoustic-structural analogy in order to use this code to perform an acoustic analysis, and finally the development of special code to deal with the actual coupling. The combined ear canal/eardrum model developed here is a preliminary model, where the simplified geometry permitted an uncomplicated initial examination of the effects of coupling. Results obtained for the ear canal as cylindrical tube coupled to the eardrum as flat plate are promising and indicate the future usefulness of the method, especially when more realistic geometry is included in the modelling.

6.2 FUTURE WORK

The next step in modelling is to include proper geometrical representation for both the eardrum and ear canal. The curved cone-like shape of the eardrum is important and must be included in the model. The eardrum's various sections, including the pars tensa, the pars flaccida and the manubrium should also be distinguished, with appropriate material properties assigned to each section. The ear canal's actual geometry must also be included. The importance of the

middle ear must also be considered, including the behaviour of the ligaments and ossicles as well as the loading effects of the middle-ear air cavities.

To begin, future work will take two different directions. In one case, work will be continued on modelling the human eardrum and ear canal, stressing a better geometrical representation of the system. However, as finite-element modelling of the cat eardrum has already been undertaken (Funnell, 1983), future work will also deal with modelling the coupled system of ear canal and eardrum for a cat. The methods that will be applied to reconstruct the three-dimensional geometry of the ear canal have already been developed. Cat ear-canal data will be generated using a series of histological slices. Each prepared slide will be projected onto a surface and contours defining the shape of the ear canal will be digitized and stored on the computer. After aligning the digitized slices, the three-dimensional geometry of the ear canal will be reconstructed. This method of three-dimensional reconstruction has been used to reconstruct the middle-ear ligaments and ossicles as described in Funnell (1989). The three-dimensional ear canal must then be meshed into elements, and this could be a complicated process. It will be undertaken using a three-dimensional meshing program for irregular shapes developed by Boubez (1985), which automatically generates a mesh of tetrahedral elements for a three-dimensional object using serial sections. This program has been successfully applied to the meshing of a cat middle-ear ligament (Funnell, 1989).

Modelling the coupled system for both cat and human can be approached using methods other than pure finite-element analysis. For example, the ear canal can be modelled using the boundary-element method, where the structure of the ear canal would be defined only by its boundary. Boundary elements are now frequently used in conjunction with finite elements; for example, in fluid-structure interaction problems, the fluid can be represented using two-dimensional surface boundary elements which match on the boundary of the finite-element mesh

of the structure (Walker, 1980; Everstine and Henderson, 1990). The advantages of modelling using these hybrid methods include simpler mesh generation and decreased computation time for some problems. High-quality commercial code which combines finite-element and boundary element methods has recently started to appear (Coyette, 1990).

6.3 APPLICATIONS

After including more accurate anatomical representations in the coupled problem, it will be possible to undertake comparisons with actual experimental data. Furthermore, it will be possible to examine how various parameters affect the behaviour of the model. For example, ear-canal length, size and shape could be altered to determine the effect on ear-canal sound pressures. Results obtained from such an analysis might then be compared with those of Goode et al. (1977), who found that modifications of external-ear anatomy following tympanomastoid surgery can have significant effects on the external ear sound-pressure gain and therefore human hearing response.

Obviously, the coupled system will have different features for different species. For example, as discussed in Chapter Two, the human, cat, and guinea-pig ear canals each have distinctive features. Other features which will differ across species, including the shape of the concha and the orientation of the eardrum, will be important in the coupled problem (Rabbitt and Holmes, 1988). Therefore, modelling the coupled system for different animals should reveal interesting information regarding the role of specific ear components and geometry in the interaction problem.

The initial finite-element modelling which has been undertaken for the cat middle-ear ligaments and ossicles (Funnell, 1989) has already been mentioned. However, to complete middle-ear modelling, the air cavities must be included, and this will involve the use of the fluid-structure coupling method developed here. Combining the resulting middle-ear model with existing eardrum models, and the ear canal/eardrum work undertaken in this thesis, it should eventually be possible to have a complete finite-element model of the middle and outer ear with appropriate structures of interest modelled as desired. Such a model would be of considerable use in understanding the transmission of sound through the eardrum and lead to a greater knowledge of the hearing process in general.

REFERENCES

- Akkas, N., Akay, H.U., and Yilmaz, C. (1979). "Applicability of general-purpose finite element programs in solid-fluid interaction problems," *Comput. Struct.*, **10**, 773-783.
- Anson, B.J. and Donaldson, J.A. (1973). Surgical Anatomy of the Temporal Bone and Ear. (W.B. Saunders, Philadelphia).
- Bathe, K.J. (1974 revised). SAP IV - A Structural Analysis Program for Static and Dynamic Response of Linear Systems. Report no. EERC 73-11, College of Engineering, University of California, (Berkeley, California).
- Bathe, K.J. (1982). Finite Element Procedures in Engineering Analysis. (Prentice-Hall, New Jersey).
- Bauer, B.B. (1965). "Equivalent circuit of a tube or spring," *J. Acoust. Soc. Am*, **38**, 882.
- Békésy, G.v. (1941). "On the measurement of the amplitude of vibration of the ossicles with a capacitive probe," *Akust. Zeitschr*, **6**, 1-16. [in German]
- Békésy, G.v. (1949). "The structure of the middle ear and the hearing of one's own voice by bone conduction," *J. Acoust. Soc. Am*, **21**, 217-232.
- Belytschko, T. (1980). "Fluid-structure interaction," *Comput. Struct*, **12**, 459-469.
- Boubez, T.I. (1986). Three-Dimensional Finite-Element Mesh Generation Using Serial Sections (M. Eng. Thesis, McGill University, Montreal).
- Brebbia, C.A., and Dominguez, J. (1989). Boundary Elements: An Introductory Course. (McGraw-Hill, NY).
- Buunen, T.J.F., and Vlaming, M.S.M.G. (1981). "Laser-Doppler velocity meter applied to tympanic membrane vibrations in cat," *J. Acoust. Soc. Am.*, **69**(3), 744-750
- Cook, R.D., and Young, W.C. (1985). Advanced Mechanics of Materials (Macmillan Publishing Company, New York).
- Coyette, J.P. (1990). "Finite element and boundary element techniques to solve acoustic problems," *Can. Acoust.*, **18**(3), 75
- Dahmann, H. (1929). "On the physiology of hearing. experimental studies on the mechanics of the ossicular chain, as well as on the behaviours of tones and air pressure I," *Zeitschr. f. Hals. Nas. Ohrenhkl.*, **24**, 462-498. [in German].

- Dahmann, H. (1930). "On the physiology of hearing: experimental studies on the mechanics of the ossicular chain, as well as on the behaviours of tones and air pressure II-IV," *Zeitschr. f. Hals. Nas. Ohrenhik.*, 27, 329-368, discussion 398-402. [in German].
- Decraemer, W.F. (1980). Personal communication to W.R.J. Funnell.
- Decraemer, W.F., Khanna, S.M., and Funnell, W.R.J. (1989). "Interferometric measurement of the amplitude and phase of tympanic membrane vibrations in cat," *Hear. Res.*, 38(1), 1-18.
- Decraemer, W.F., Khanna, S.M., and Funnell, W.R.J. (1990). "Heterodyne interferometer measurements of the frequency resonance of the manubrium tip in cat," *Hear. Res.*, 47(3), 205-217.
- Esser, M.H.M. (1947). "The mechanism of the middle ear: II. The drum," *Bull. Math. Biophys.*, 9, 75-91.
- Everstine, G.C., and Henderson, (1990). "Coupled finite element/boundary element approach for fluid-structure interaction," *J. Acoust. Soc. Am.*, 87(5), 1938-1947.
- Everstine, G.C., Henderson, F.M., and Lipman, R.R. (1984). "Finite element prediction of acoustic scattering and radiation from submerged elastic structures," Proceedings of Twelfth NASTRAN User's Colloquium, NASA Conference Publication 2328, 192-209.
- Everstine, G.C., Schroeder, E.A., and Marcus, M.S. (1975). "The dynamic analysis of submerged structures," Proceedings of the Fourth NASTRAN User's Colloquium, NASA TM X-3278, 419-429.
- Fung, Y.C. (1981). Biomechanics - Mechanical Properties of Living Tissues. (Springer, New York).
- Funnell, S. (1989). An Approach to Finite-Element Modelling of the Middle Ear. (Master's Thesis, McGill University, Montréal).
- Funnell, W.R.J. (1972). The Acoustical Impedance of the Guinea-Pig Middle Ear and the Effects of the Middle-Ear Muscles. (Master's Thesis, McGill University, Montréal).
- Funnell, W.R.J. (1975) A Theoretical Study of Eardrum Vibrations Using the Finite-Element Method. (PhD Thesis, McGill University, Montréal).
- Funnell, W.R.J. (1983). "On the undamped natural frequencies and mode shapes of a finite-element model of the cat eardrum," *J. Acoust. Soc. Am.*, 73(5), 1657-1661.
- Funnell, W.R.J., Decraemer, W.F., and Khanna, S.M. (1987). "On the damped frequency response of a finite-element model of the cat eardrum," *J. Acoust. Soc. Am.*, 81, 1851-1859.

- Funnell, W.R.J., and Laszlo, C.A. (1978). "Modelling of the cat eardrum as a thin shell using the finite-element method," *J. Acoust. Soc. Am.*, **63**, 1461-1467.
- Funnell, W.R.J., and Laszlo, C.A. (1982). "A critical review of experimental observations on eardrum structure and function," *ORL*, **44**(4), 181-205.
- Gardner, M.B., and Hawley, M.S. (1972). "Network representation of the external ear," *J. Acoust. Soc. Am.*, **52**(6), 1620-1628.
- Gardner, M.B., and Gardner, R.S. (1973). "Problem of localization in the median plane: effect of pinnae cavity occlusion," *J. Acoust. Soc. Am.*, **53**(2), 400-408.
- Goode, R.L., Friedrichs, R., and Falk, S. (1977). "Effect on hearing thresholds of surgical modification of the external ear," *Ann. Otol. Rhinol. Laryngol.*, **86**(4), 441-451.
- Grandin, H. (1986). Fundamentals of the Finite Element Method. (Macmillan, New York).
- Guinan, J.J., and Peake, W.T. (1967). "Middle-ear characteristics of anesthetized cats," *J. Acoust. Soc. Am.*, **41**(5), 1237-1261.
- Hamdi, M.A., and Ousset, Y. (1978). "A displacement method for the analysis of vibrations of coupled fluid-structure systems," *Int. J. Num. Meth. in Engrg.*, **13**, 139-150.
- Harkness, R.D. (1961). "Biological functions of collagen," *Biol. Rev. Cambridge Phil. Soc.*, **36**, 399-463.
- Helmholtz, H.L.F. (1869). "The mechanism of the middle-ear ossicles and of the eardrum," *Pfügers Arch. f. Physiol. (Bonn)*, **1**(1-60). [in German].
- Hildebrand, F.B. (1968). Finite Difference Equations and Simulations (Prentice-Hall, N.J.).
- Hudde, H. (1983). "Estimation of the area function of human ear canals by sound pressure measurement," *J. Acoust. Soc. Am.*, **73**(1), 24-31.
- Johansen, P.A. (1975). "Measurement of the human ear canal," *Acustica*, **33**(5), 349-351.
- Kalinowski, A.J., and Nebelung, C.W. (1982). "Solution of axisymmetric fluid structure interaction problems with NASTRAN," Proceedings of Tenth NASTRAN User's Colloquium, NASA Conference Publication 2249, 87-111
- Kessel, J. (1874). "On the influence of the middle-ear muscles on the displacements and vibrations of the eardrum in the cadaver ear," *Arch. Ohrenhkl.*, **8**, 80-92 [in German]
- Khanna, S.M. (1970). A Holographic Study of Tympanic Membrane Vibrations in Cats (PhD Thesis, City University of New York, NYC).

- Khanna, S.M., and Stinson, M.R. (1985). "Specification of the acoustical input to the ear at high frequencies," *J. Acoust. Soc. Am.*, **77**(2), 577-589.
- Khanna, S.M., and Stinson, M.R. (1986). "Sound pressure distribution in the ear canals of cats," in Proceedings of the 12th International Congress on Acoustics, Toronto, Canada, paper B6-4.
- Khanna, S.M., and Tonndorf, J. (1969). "Middle ear power transfer," *Arch. klin. exp. Ohr. Nas. Kehlk. Heilk.*, **193**, 78-88.
- Khanna, S.M., and Tonndorf, J. (1972). "Tympanic membrane vibrations in cats studied by time-averaged holography," *J. Acoust. Soc. Am.*, **51**, 1904-1920.
- Kirikae, I. (1960). The Structure and Function of the Middle Ear. (University of Tokyo Press, Tokyo).
- Kobrak, H.G. (1941). "A cinematographic study of the conduction of sound in the human ear," *J. Acoust. Soc. Am.*, **13**, 179-181.
- Kohnke, P.C. (1977). ANSYS Engineering Analysis System Theoretical Manual (Swanson Analysis Systems, Houston, PA).
- Kojo, Y. (1954). "Morphological studies of the human tympanic membrane," *J. O.-R.-L. Soc. Japan*, **57**, 115-126. [in Japanese].
- Lamancusa, J.S. (1988). "Acoustic finite element modeling using commercial structural analysis programs," *J. Noise Cont. Eng.*, **30**(2), 65-71.
- Lawton, B.W., and Stinson, M.R. (1986). "Standing wave patterns in the human ear canal used for estimation of acoustic energy reflectance at the eardrum," *J. Acoust. Soc. Am.*, **79**(4), 1003-1009.
- Lim, D.J. (1970). "Human tympanic membrane," *Acta Otolaryngol.*, **70**, 176-186.
- Lynch, T.J. (1981). Signal Processing By the Cat Middle Ear: Admittance and Transmission, Measurements and Models. (PhD Thesis, Massachusetts Institute of Technology, Cambridge, Mass.)
- Mader, L. (1900). "Microphonic studies of the sound-conducting apparatus of the human ear," *SitzBer. Math.-Naturw. Cl. Kaiser. Akad. Wiss. (Wien)* **3**, 109, 37-75. [in German].
- Møller, A.R. (1963). "Transfer function of the middle ear," *J. Acoust. Soc. Am.*, **35**(10), 1526-1534.
- Møller, A.R. (1961). "Network model of the middle ear," *J. Acoust. Soc. Am.*, **33**(6), 794-805.

- Morse, P.M., and Ingard, K.U. (1968). Theoretical Acoustics. (McGraw-Hill, NY).
- Numerical Algorithms Group (1988). NAG Fortran Library Manual - Mark 13. (NAG Inc., Downers Grove, Ill.).
- Olson, L.G., and Bathe, K.J. (1985). "Analysis of fluid-structure interactions. A direct symmetric coupled formulation based on the fluid velocity potential," *Comput. Struct.*, **21**, 21-32.
- Onchi, Y. (1961). "Mechanism of the middle ear," *J. Acoust. Soc. Am.*, **33**(6), 794-805.
- Perlman, H.B. (1945). "Stroboscopic examination of the ear," *Ann. O.R.L.*, **54**, 483-494.
- Rabbitt, R.D. (1985). "A dynamic fiber composite continuum model of the tympanic membrane. Part I: Model Formulation," Math. Report No. 151. (Rensselaer Polytechnic Institute, Troy, NY).
- Rabbitt, R.D. (1988). "High-frequency plane waves in the ear canal: Application of a simple asymptotic theory," *J. Acoust. Soc. Am.*, **84**(6), 2070-2080.
- Rabbitt, R.D. (1990). "A hierarchy of examples illustrating the acoustic coupling of the eardrum," *J. Acoust. Soc. Am.*, **87**(6), 2566-2582.
- Rabbitt, R.D., and Holmes, M.H. (1986). "A fibrous dynamic continuum model of the tympanic membrane," *J. Acoust. Soc. Am.*, **80**(6), 1716-1728.
- Rabbitt, R.D., and Holmes, M.H. (1988). "Three-dimensional acoustic waves in the ear canal and their interaction with the tympanic membrane," *J. Acoust. Soc. Am.*, **83**(3), 1064-1080.
- Roffler, S.K., and Butler, R.A. (1968). "Factors that influence the localization of sound in the vertical plane," *J. Acoust. Soc. Am.*, **43**(6), 1255-1259.
- Shaw, E.A.G. (1974). "The external ear," in Handbook of Sensory Physiology, edited by W.D. Keidel and W.D. Neff (Springer-Verlag, Berlin), Vol. v/1, Chap. 14, pp. 455-490.
- Shaw, E.A.G. (1975). "The external ear: new knowledge," in Earmoulds and Associated Problems (Proc. Seventh Danavox Symposium, GL. Avernoes, Denmark), *Scand. Audio. Suppl.* 5, pp. 24-50.
- Shaw, E.A.G. (1977). "Eardrum representation in middle-ear acoustical networks," *J. Acoust. Soc. Am. Suppl.* 1, **62**, S12.
- Shaw, E.A.G. (1980). "The acoustics of the external ear," in Acoustical Factors Affecting Hearing Aid Performance, edited by G.A. Studebaker and I. Hochberg (University Park, Baltimore), pp. 109-125.

- Shaw, E.A.G., and Stinson, M.R. (1981). "Network concepts and energy flow in the human middle-ear," *J. Acoust. Soc. Am. Suppl. 1*, **69**, S43.
- Shaw, E.A.G., and Stinson, M.R. (1986). "Eardrum dynamics, middle ear transmission and the human hearing threshold curve," *Proceedings of the 12th International Congress on Acoustics, Toronto*, paper b6-6.
- Shaw, E.A.G., and Teranishi, R. (1968). "Sound pressure generated in an external-ear replica and real human ears by a nearby point source," *J. Acoust. Soc. Am.*, **44**(1), 240-249.
- Sinyor, A. (1971). A Theoretical and Experimental Investigation of the Acoustic Transmission Properties of the External Ear. (Master's Thesis, McGill University, Montréal).
- Sinyor, A., and Laszlo, C.A. (1973). "Acoustic behaviour of the outer ear of the guinea pig and the influence of the middle ear," *J. Acoust. Soc. Am.*, **54**(4), 916-921.
- Stinson, M.R. (1985a). "Spatial variation of phase in ducts and measurement of acoustic energy reflection coefficients," *J. Acoust. Soc. Am.*, **77**(2), 386-393.
- Stinson, M.R. (1985b). "The spatial distribution of sound pressure within scaled replicas of the human ear canal," *J. Acoust. Soc. Am.*, **78**(5), 1596-1602.
- Stinson, M.R., and Khanna, S.M. (1989). "Sound propagation in the ear canal and coupling to the eardrum, with measurements on model systems," *J. Acoust. Soc. Am.*, **85**(6), 2481-2491.
- Stinson, M.R., and Lawton, B.W. (1989). "Specification of the geometry of the human ear canal for the prediction of sound-pressure level distribution," *J. Acoust. Soc. Am.*, **85**(6), 2492-2503.
- Stinson, M.R., and Shaw, E.A.G. (1982). "Wave effects and pressure distribution in the human ear canal," *J. Acoust. Soc. Am. Suppl. 1*, **71**, S88.
- Stinson, M.R., and Shaw, E.A.G. (1983). "Sound pressure distribution in the human ear canal," *J. Acoust. Soc. Am. Suppl. 1*, **73**, S59-60.
- Stinson, M.R., Shaw, E.A.G., and Lawton, B.W. (1982). "Estimation of acoustical energy reflectance at the eardrum from measurements of pressure distribution in the human ear canal," *J. Acoust. Soc. Am.*, **72**(3), 766-773.
- Teranishi, R., and Shaw, E.A.G. (1968). "External-ear acoustic models with simple geometry," *J. Acoust. Soc. Am.*, **44**(1), 257-263.
- Tonndorf, J., and Khanna, S.M. (1972). "Tympanic-membrane vibrations in human cadaver ears studied by time-averaged holography," *J. Acoust. Soc. Am.*, **52**, 1221-1233.

- Vander, A.J., Sherman, J.H., and Luciano, D.S. (1985). Human Physiology - The Mechanisms of Body Function. (McGraw-Hill, NY).
- Walker, S. (1980). "Boundary elements in fluid-structure interaction problems," *Appl. Math. Modelling*, **4**, 345-350.
- Weiner, F.M., Pfeiffer, R.R., and Backus, A.S. (1965). "On the sound pressure transformation by the head and auditory meatus of the cat," *Acta. Otolaryngol.*, **61**, 255-269.
- Weiner, F.M. and Ross, D.A. (1946). "The pressure distribution in the auditory canal in a progressive sound field," *J. Acoust. Soc. Am.*, **18(2)**, 401-408.
- Wever, E.G. and Lawrence, M. (1954). Physiological Acoustics. (Princeton University Press, New Jersey).
- Zienkiewicz, O.C., and Bettess, P. (1978). "Fluid-structure dynamic interaction and wave forces. An introduction to numerical treatment," *Int. J. Num. Meth. Engng.*, **13**, 1-16.
- Zwislocki, J. (1962). "Analysis of the middle-ear function. Part I: Input impedance," *J. Acoust. Soc. Am.*, **34(9)**, 1514-1523.
- Zwislocki, J. (1965). "Analysis of Some Auditory Characteristics," in Handbook of Mathematical Psychology, edited by R.D. Luce, R.R. Bush, and E. Galanter, (Wiley, NY).
- Zwislocki, J. (1970). "An Ear-like coupler for earphone calibration," LSC-S-9 Grant NGR-33-022-091, Nat. Aeron. Space Admin., Washington D.C. 20546. (From the Laboratory of Sensory Communication, Syracuse University, N.Y. 13210.) [as cited by Gardner and Hawley, 1972].